Photoprotection is regulated by light-independent CO_2 availability

Short title: CO_2 availability controls photoprotection

Authors

M. Águila Ruiz-Sola[1,†,‡], Serena Flori[1,†], Yizhong Yuan[1,†], Gaelle Villain[1], Emanuel Sanz-Luque[2,3], Petra Redekop[2], Ryutaro Tokutsu[4], Anika Kueken[5,6], Angeliki Tsichla[1], Georgios Kepesidis[1], Guillaume Allorent[1], Marius Arend[5,6], Fabrizio Iacono[1], Giovanni Finazzi[1], Michael Hippler[7], Zoran Nikoloski[5,6], Jun Minagawa[4], Arthur R. Grossman[2], Dimitris Petroutsos[1,*]

Affiliations

[1]Univ. Grenoble Alpes, CNRS, CEA, INRAE, IRIG-LPCV, 38000 Grenoble, FRANCE
[2]The Carnegie Institution for Science, Department of Plant Biology, Stanford, CA 94305, USA
[3]University of Cordoba, Department of Biochemistry and Molecular Biology, Cordoba, SPAIN
[4]Division of Environmental photobiology, National Institute for Basic Biology (NIBB), Nishigonaka 38, Myodaiji, Okazaki 444-8585, JAPAN
[5]Bioinformatics Group, Institute of Biochemistry and Biology, University of Potsdam, Potsdam, GERMANY.
[6]Max-Planck-Institute of Molecular Plant Physiology, Potsdam, Golm, GERMANY
[7]Institute of Plant Biology and Biotechnology, Westfälische Wilhelms Universität, 48143 Münster, GERMANY

[†] these authors contributed equally to this work

[‡] Current address: Instituto de Bioquímica Vegetal y Fotosíntesis, Universidad de Sevilla-CSIC, 41092, Sevilla, SPAIN

[*]Corresponding Author. Email: *dimitris.petroutsos@cea.fr*

Abstract

Photosynthetic algae cope with suboptimal levels of light and CO_2. In low CO_2 and excess light, the green alga *Chlamydomonas reinhardtii* activates a CO_2 Concentrating Mechanism (CCM) and photoprotection; the latter is mediated by LHCSR1/3 and PSBS. How light and CO_2 signals converge to regulate photoprotective responses remains unclear. Here we show that excess light activates expression of photoprotection- and CCM-related genes and that depletion of CO_2 drives these responses, even in total darkness. High CO_2 levels, derived from respiration or impaired photosynthetic fixation, repress *LHCSR3* and CCM genes while stabilizing the LHCSR1 protein. We also show that CIA5, which controls CCM genes, is a major regulator of photoprotection, elevating *LHCSR3* and *PSBS* transcript accumulation while inhibiting LHCSR1 accumulation. Our work emphasizes the importance of CO_2 in regulating photoprotection and the CCM, demonstrating that the impact of light on photoprotection is often indirect and reflects intracellular CO_2 levels.

Teaser

Photoprotection- and CCM-related genes can be activated by changes in CO_2 availability even in the absence of light.

Keywords

Photosynthesis, photoprotection, energy dependent quenching qE, CO_2, LHCSR, PSBS, CO_2-concentrating mechanism (CCM), CIA5/CCM1, *Chlamydomonas*

Introduction

A major challenge for photosynthetic organisms is to efficiently acclimate to the highly dynamic light and nutrient conditions that occur in their natural environments. While light provides the energy that fuels photosynthetic CO_2 fixation, excess light causes oxidative damage and ultimately result in cell death. Therefore, light absorption must be precisely managed, via photoprotective mechanisms that integrate the use of light energy with CO_2 availability and the potential of the organism to grow and store fixed carbon. A dominant photoprotective mechanism, called qE (energy dependent quenching), results in harmless dissipation of excess absorbed light energy as heat[1,2]. Triggering qE requires the synthesis of specific proteins and pigments that are controlled both transcriptionally and post-transcriptionally.

In the green microalga *Chlamydomonas reinhardtii* (hereafter *Chlamydomonas*), qE depends on the nucleus-encoded, chloroplast-localized Light Harvesting Complex-Stress Related proteins LHCSR1, LHCSR3 and Photosystem II Subunit S, PSBS, which are present in many algae and lower plants[3] and belong to the Light Harvesting Complex protein superfamily[4]. The *LHCSR3.1* and *LHCSR3.2* genes in *Chlamydomonas* encode identical LHCSR3 proteins[5], while *PSBS1* and *PSBS2* encode PSBS proteins that differ only in one amino acid of the chloroplast transit peptide[6]. While LHCSR1 and LHCSR3 are present in algae but not in vascular plants, PSBS is present in both[4]. PSBS in *Chlamydomonas* is transiently expressed in cells exposed to high light (HL)[6,7] and accumulates in cells exposed to UV-B irradiation[8]. LHCSR3 is the main qE effector protein in HL[5], although LHCSR1 can significantly contribute to qE under certain conditions[9]. In *Chlamydomonas*, expression of *LHCSR3* has been reported to increase upon absorption of blue-light by the photoreceptor phototropin (PHOT1)[10] and involves calcium ion signaling[11], active photosynthetic electron transport[10,11] and the transcriptional factor CONSTANS, which is also required for activation of the *LHCSR1* and *PSBS* genes[12,13].

Similar to the dynamic character of the light environment, the concentration of inorganic carbon (HCO_3^-, CO_2 and CO_3^{2-}, together designated Ci) in aquatic environments varies spatially and temporally; aquatic CO_2 levels can also fluctuate from extremely high (hyper-saturated) to extremely low[14]. Because low CO_2 levels can limit photoautotrophic growth, microalgae have evolved a CO_2 concentrating mechanism (CCM) that elevates the level of CO_2 at the site of fixation by RuBisCo. Major components of the CCM are carbonic anhydrases (CAH), which facilitate interconversions among the different Ci species, and Ci transporters. The genes encoding many Ci transporters and CAHs are under the control of the zinc-finger type transcription regulator CIA5 (also CCM1)[15,16], which is localized in the nucleus[17] and controls the expression of low-CO_2 responsive genes.

In addition to the use of CO_2 to support phototrophic growth in the light, *Chlamydomonas* is also able to use the two-carbon molecule acetate either in the dark to support heterotrophic growth, or in the light, to support photoheterotrophic or mixotrophic growth[18]. Acetate is incorporated into acetyl-CoA either as a one-step reaction, catalyzed by acetyl-CoA synthetase (ACS), or in two steps in which acetate kinase (ACK) and phosphate acetyltransferase (PAT) sequentially catalyze the formation of acetyl-phosphate and acetyl-CoA[19]. Acetyl-CoA can then enter the glyoxylate cycle, a shunt of the tricarboxylic acid (TCA) cycle[20] recently characterized in Chlamydomonas [21], where it can be converted to metabolites that are used for anabolic metabolism. Alternatively, acetyl-CoA enters the TCA cycle to feed the respiratory chain with reducing equivalents. Both the glyoxylate cycle and respiration are essential for growth in the dark since *Chlamydomonas* mutants affected in either of these processes are unable to grow heterotrophically[21,22].

Despite the evident connection between light and CO_2 levels, the physiological responses to different light and CO_2 availabilities have been traditionally studied separately. However, several lines of evidence indicate that both acetate and Ci abundance impact not only qE but also the

establishment of the CCM in *Chlamydomonas*. Acetate, the preferred source of fixed carbon for *Chlamydomonas* mixotrophic growth, can suppress CCM induction[23,24] and also inhibits LHCSR3 protein accumulation in cells exposed to relatively HL[25]. Acetate also alters the functional features of photosystem II rendering it less susceptible to photoinhibition[26]. Like acetate, excess CO_2 also supresses *LHCSR3* expression [27] and protein accumulation [25] under similar light conditions. On the other hand, *LHCSR3* transcript accumulation can be elicited by exposure of cells to low CO_2 in low light (LL) in a CIA5-dependent manner [27,28]. The mechanism(s) associated with carbon-dependent regulation of *LHCSR3* and the intimate link between acetate metabolism and the CCM have still not been clearly defined.

Here, using genetic, transcriptomic and mathematical modelling approaches, we demonstrate that the inhibition of LHCSR3 accumulation and CCM activity by acetate is at the level of transcription and a consequence of metabolically produced CO_2. We show that exposure of *Chlamydomonas* to HL triggers not only HL-responses, but also low-CO_2 responses, and we report the discovery of a novel CO_2- and CIA5-dependent pathway that activates *LHCSR3* gene expression even in complete darkness. Finally, we propose that photosynthetic electron flow is critical for activation of *LHCSR3* transcription because it sustains CO_2 fixation, consuming intracellular CO_2 and thereby relieving its inhibitory effect. This work emphasizes the critical importance of intracellular CO_2 levels in regulating *LHCSR3* expression and how light mediated responses may be indirect and reflect changes in internal CO_2 levels resulting from light intensity dependent, photosynthetic fixation of intracellular CO_2.

Results

LHCSR3 transcript accumulation is impacted by acetate metabolism

To gain insights into the effect of carbon metabolism on photoprotection, we initially explored the impact of acetate and high CO_2 on *LHCSR3* mRNA and protein levels. Wild type (WT) cells were acclimated overnight in High Salt Medium (HSM) in LL sparged with air, in the presence or absence of acetate, or sparged with 5% CO_2. Following this acclimation period, the cells were transferred from LL to HL, with all other conditions identical to those of the acclimation period. Samples were collected after 1 h for RNA analyses and after 4 h for protein analysis and measurements of photosynthetic activity. The presence of acetate in the medium of WT cells for both the overnight LL acclimation and the HL treatment, inhibited accumulation of the *LHCSR3* transcript (**Fig. 1a**, note the logarithmic scale). No protein was detected under any condition in LL, but inhibition by acetate was apparent in HL (**Fig. 1b**). Using the same protocol, we examined how acetate and CO_2 impacted the HL-elicited accumulation of the LHCSR3 transcript and protein in two mutants which are impaired in acetate metabolism and have slower growth under heterotrophic and mixotrophic conditions than WT cells; the *icl* mutant, which lacks isocitrate lyase, a key enzyme of the glyoxylate cycle[21], and the *dum11* mutant, which is defective in ubiquinol cytochrome c oxidoreductase of the respiratory complex III[29]. In the *icl* mutant, unlike in WT cells, acetate had no inhibitory effect on accumulation of LHCSR3 mRNA (**Fig. 1a**) or protein (**Fig. 1b**) in either HL or LL, while the *icl::ICL*-complemented line, designated *icl-C*, behaved similarly to WT cells (**Fig. 1a** and **b**); similar trends were observed in WT and the complemented strain, although the absolute values were somewhat different. Furthermore, under HL conditions, unlike WT cells, acetate did not alter LHCSR3 transcript or protein accumulation in the *dum11* mutant (**Fig. 1c and d)**, while under LL, acetate inhibited *LHCSR3* transcript in the *dum11* mutant to a much smaller extent than in WT (**Fig. 1c)**. Additionally, LHCSR3 protein appeared to be slightly higher in both *dum11* and *icl* mutants under LL conditions (see the faint LHCSR3 bands in **Fig. 1b** and **d**, LL panel**)**. Together, these results suggest that the acetate administered to the cells must be metabolized for it to have a suppressive effect on accumulation of LHCSR3 transcript and protein in HL.

CO_2 generated from acetate metabolism inhibits accumulation of LHCSR3 transcript and protein

We also sparged WT, *icl, icl-C* and *dum11* cells with 5% CO_2 during both acclimation and exposure to HL. CO_2 strongly repressed accumulation of *LHCSR3* mRNA and protein in all genotypes in HL, including the metabolic mutants *icl* and *dum11* for which expression of *LHCSR3* was unaffected by acetate (**Fig. 1a-d)**. As mentioned earlier, the *icl* mutant appeared to accumulate low levels of LHCSR3 protein under LL air conditions where LHCSR3 was not detectable in WT (**Fig. 1b**). We could also detect LHCSR3 accumulation in *icl* cells sparged with 5% CO_2 under LL **(Fig. 1b).** We attribute this result to the fact that prior to the acclimation period of this experiment, cells were maintained in TAP in LL (mixotrophy), conditions that would favor some accumulation of LHCSR3 protein in *icl* cells[21] but not in WT cells. Given the long half-life of the LHCSR3 protein[30], it is likely that the 16 h pretreatment in LL was not enough time to allow for complete turnover of the LHCSR3 that had accumulated, even in the case of sparging with 5% CO_2, which strongly repressed accumulation of LHCSR3 protein in all genotypes in HL (**Fig. 1b**).

The similarity between the impact of acetate and 5% CO_2 on expression of *LHCSR3* in WT and *icl-C* cells raised the possibility that both treatments elicited a common mechanism by which *LHCSR3* is controlled, possibly by altering the concentration of CO_2 within the cell or in the growth medium. This possibility is plausible based on the finding that acetate metabolism leads to the generation of CO_2, as previously shown by radiotracer and CO_2-electrode based approaches[31]. To investigate whether the generation of CO_2 via acetate metabolism can explain the repression of *LHCSR3* transcript and protein levels, we monitored the levels of transcripts from the *RHP1* gene in the mutant and WT cells; *RHP1* (aka *RH1*) encodes a CO_2 channel shown to be CO_2 responsive and to accumulate in cells growing in a high CO_2 atmosphere[32]. WT and *icl* mutant cells were acclimated overnight in HSM LL sparged with air ("air" conditions, as indicated in the legend of **Fig. 2**) followed by the introduction of acetate or 5% CO_2 (t =0); the cells were assayed for the levels of the *LHCSR3* and *RHP1* transcripts over a period of 8 h in LL (**Fig. 2a** and **b**). The *LHCSR3* transcript accumulation patterns observed agreed with the findings presented in **Fig. 1a** (Low Light panel). In WT cells, acetate and CO_2 caused a reduction in *LHCSR3* mRNA accumulation over the LL period relative to the control (no acetate, air). On the other hand, in the *icl* mutant, acetate did not affect accumulation of this transcript while CO_2 efficiently repressed the *LHCSR3* transcript level (**Fig. 2a**). Under these experimental conditions, acetate levels in the medium decreased in WT cultures but remained unchanged in cultures of the *icl* mutant over the course of the experiment (**Fig. 2c**). Finally, when we assessed intracellular CO_2 levels by using *RHP1* transcript levels as a proxy, we found that expression of this gene increased in WT cells when the culture was sparged with CO_2 or supplemented with acetate, suggesting that acetate metabolism led to higher intracellular CO_2 levels. In contrast, in *icl* mutant cells, *RHP1* gene expression increased when the cultures were sparged with CO_2 but not when supplemented with acetate (**Fig. 2b**).

In a separate experiment, cells acclimated overnight in HSM LL sparged with air were shifted to HL (t=0) and we assayed *LHCSR3* and *RHP1* transcript levels over a period of 9 h; acetate or high CO_2 were introduced 1 h after the shift to HL (**Fig. 2d** and **e**, note the 1 h time point highlighted in green on the x axis). In agreement with **Fig. 1** (High Light panel), *LHCSR3* transcript accumulation increased by two orders of magnitude after 1 h exposure to HL in both WT and the *icl* mutant (**Fig. 2d**), while *RHP1* transcripts rapidly decreased **(Fig. 2e)**, likely a consequence of enhanced CO_2 assimilation resulting from increased photosynthetic CO_2 fixation. Introduction of acetate or CO_2 to the cultures caused a rapid reduction in the level of *LHCSR3* expression in WT (**Fig. 2d**), with the decline much more pronounced with CO_2 supplementation. Supplementation with acetate also caused an increase of *RHP1* transcript relative to the control. In contrast, in the *icl* mutant, the decline in the level of the *LHCSR3* transcript and the increase in the level of the *RHP1* transcript

was the same in cells with and without acetate supplementation, while the effect of CO_2 was similar as in WT cells (**Fig. 2d** and **e**). Furthermore, as shown in **Fig. 2f**, like in **Fig. 2c**, the WT cells consumed about half of the acetate in the medium over the course of the experiment while none of the acetate was consumed by the *icl* mutant. These results strongly support the hypothesis that CO_2 inhibits accumulation of the *LHCSR3* transcript and that the decline in the level of *LHCSR3* mRNA in WT cells supplemented with acetate is a consequence of the CO_2 released as the acetate is metabolized. The extent of this inhibition by acetate-derived CO_2 appears to depend mostly on the rate of photosynthetic CO_2 fixation (consumption of CO_2) because acetate was taken up by WT cells at similar rates under both LL and HL conditions (**Fig. 2c** and **f**). Indeed, under LL conditions, where CO_2 fixation is slow, acetate and CO_2 repressed *LHCSR3* to the same extent (**Fig. 2a**); under HL conditions, where CO_2 fixation is much faster, the effect of acetate on the *LHCSR3* transcript level is much smaller than that of CO_2 (**Fig. 2d**).

We also employed genome-scaled metabolic modelling to assess *in silico* whether acetate metabolism in *Chlamydomonas* leads to an increase in the concentration of intracellular CO_2 under different growth conditions (**Supplementary Note, Supplementary Fig. 1, Supplementary Tables 1 and 2, Supplementary Data 1**). This approach supports the hypothesis that there are changes in the internal CO_2 concentration under autotrophic and mixotrophic growth conditions at different light intensities. These changes are congruent with the changes in the accumulation of *LHCSR3* transcripts under the different media conditions and in the WT and mutant cells.

Impact of carbon availability on other qE effectors

We also evaluated the impact of carbon availability on the photosynthetic properties of the cells. The presence of acetate in the medium of WT cells enhanced photosynthetic electron transport (rETR) and strongly suppressed energy dependent quenching, qE (Supplementary **Fig. 2**). In the *icl* mutant, acetate enhanced the extent of rETR only by ca. 10% compared with 60% for WT cells. Additionally, acetate caused less pronounced suppression of qE in *icl* (by 40%) compared with suppression caused in WT cells (by 95%); the *icl::ICL*-complemented line, *icl-C*, behaved similarly to WT cells (Supplementary **Fig. 2**). As expected, CO_2 enhanced rETR and suppressed qE for WT, *icl* and *icl-C* (Supplementary **Fig. 2**). Although we did not detect any acetate uptake in the *icl* mutant under our experimental conditions (**Fig. 2c** and **f**), it is likely that small amounts of acetate, undetectable by our quantification method, are taken up by the mutant, triggering the above-mentioned effects on the photosynthetic properties of *icl* (Supplementary **Fig. 2**). This would be in accordance with the findings that *icl* metabolizes acetate but at slower rates than WT cells [21]. The similarity between the impact of acetate and CO_2 on photosynthetic properties in WT and *icl-C* cells validates our findings (**Fig. 2** and **Supplementary Fig. 1**) that acetate metabolism leads to an increase in the concentration of intracellular CO_2.

As mentioned earlier, WT cells exposed to HL in the presence of acetate accumulated very little LHCSR3 protein, while in the presence of 5% CO_2, LHCSR3 was not readily detected (**Fig. 1b**). Interestingly, qE levels did not correlate with LHCSR3 protein levels; cells grown in the presence of acetate exhibited much lower qE compared to cells grown with 5% CO_2 sparging (Supplementary **Fig. 2b**). We reasoned that the different qE levels could correlate to different levels of the LHCSR1 protein, which also is able to quench excess light energy [5]. We probed for LHCSR1 protein levels in HL-acclimated WT cells (in whole-cell extracts used for LHCSR3 immunodetection in **Fig. 1b**; HL panel). The results showed that the pattern of LHCSR1 accumulation was different from that of LHCSR3 (Supplementary **Fig. 3a**); at variance with LHCSR3, the presence of acetate or CO_2 in the culture medium favored accumulation of the LHCSR1 protein, with CO_2 having a stronger impact on LHCSR1 accumulation compared to acetate (Supplementary **Fig. 3a**). Therefore, the higher accumulation of LHCSR1 protein could account for the higher qE levels under conditions

of elevated CO_2. We also took into consideration the impact of the protonation state of LHCSR proteins on the activation of qE [9,33]; it was recently shown that bicarbonate leads to LHCSRs deprotonation in HL-acclimated cells because part of the trans-thylakoid proton motive force is used by bestrophin-like C_i transporters [34,35]. We took HL-acclimated cells that typically accumulate both LHCSR3 and LHCSR1 proteins (as for instance in Supplementary **Fig. 3a**) and performed photosynthetic measurements in the absence or presence of 20 mM sodium bicarbonate; the bicarbonate addition was just before performing the photosynthetic measurements. As expected, bicarbonate enhanced rETR (Supplementary **Fig. 3b**) and, in line with [34], almost completely suppressed qE despite the fact under the experimental conditions both LHCSR3 and LHCSR1 typically accumulate in the cells (as in Supplementary **Fig. 3**). Together, these results suggest that CO_2-sparged cells showed higher qE than acetate-acclimated cells (Supplementary **Fig. 2b**) because part of the CO_2 would leak out of the cells during the photosynthetic measurements. Contrary to the case of CO_2, acetate remained present in the cell suspensions and kept being metabolized during the photosynthetic measurements, constantly providing an intracellular CO_2 level that suppresses qE at very low levels.

Motivated by the different protein accumulation patterns of LHCSR3 and LHCSR1 (Supplementary **Fig. 3a**) we performed additional experiments to provide more detail concerning LHCSR1 regulation. *Chlamydomonas* cells were acclimated overnight at LL in HSM sparged with air. Samples of the cultures were collected at the end of this LL acclimation period (t=0) before the light intensity was raised for each culture to 600 µmol photons m^{-2} s^{-1} (HL), sparged with air or 5% CO_2, and the mRNA and protein levels were quantified over a 25-h period. Upon initial exposure to HL, *LHCSR1* mRNA rapidly increased (2 orders of magnitude in 1 h) and then decreased to the initial level (between 4 and 8 h), in agreement with a previous report [36], in the presence or absence of high CO_2 (**Fig. 3a**). In contrast, the presence of high CO_2 sustained high levels of LHCSR1 protein over the 25-h incubation period relative to cultures maintained at ambient levels of CO_2; at ambient CO_2 the protein levels were lower at all time points, with a strong decrease between 4 and 25 h following the imposition of HL (**Fig. 3b**). These results suggest that elevated CO_2 either promotes translation of *LHCSR1* mRNA or is involved in stabilizing the protein once it is synthesized. This increased level of LHCSR1 protein under high CO_2 conditions was also noted for the results presented in **Supplementary Fig. 3a**. This contrasts with the behaviour of LHCSR3 for which there was a strong correlation between the level of mRNA and protein (the RNA was 3 orders of magnitude lower in 5% CO_2 and the protein was no longer detected) (**Fig. 3**). The kinetics of *PSBS* transcript accumulation in HL very much resemble those of *LHCSR1*, with CO_2 not having a strong impact on transcript accumulation **(Fig. 3a)**. PSBS protein accumulation could not be evaluated because it was not detectable under the experimental conditions used.

CCM1/CIA5 links HL and low CO_2 responses

The responses to HL and low CO_2 have been traditionally studied separately, despite several lines of evidence suggesting that they are integrated [27,28,37]. To elucidate the molecular connection between photoprotection and CCM, we analyzed mRNA accumulation from the CCM genes encoding LCIB and LCIE (involved in CO_2 uptake), HLA3, LCI1, CCP1, CCP2, LCIA, BST1 (Ci transporters), CAH1, CAH3, CAH4 (carbonic anhydrases) and the nuclear regulator LCR1, all previously shown to be strongly expressed under low CO_2 conditions (see [38] for a review on the roles of each of these proteins and [35] for the more recently discovered BST1). When WT, *icl* and *icl-C* strains LL acclimated cells were exposed to HL for 1 h (experiment described in **Fig. 1**) we observed a dramatic increase in CCM transcript levels in WT cells maintained in HSM; this increase was strongly suppressed when the cultures were sparged with 5% CO_2 in air and also, but to a lesser extent, in HSM supplemented with acetate. Furthermore, acetate did not cause a decline in mRNA levels in the *icl* mutant (**Fig. 4a** and **Supplementary Fig. 4**). This pattern of mRNA accumulation from several of the CCM genes was essentially identical to that of *LHCSR3* (**Fig. 1a**), namely

suppressed levels in both acetate and high CO_2, with the impact of acetate eliminated in the *icl* mutant. The CO_2-mediated repression was more pronounced for most of the CCM genes relative to *LHCSR3* (**Fig. 1a, Fig. 4a** and **Supplementary Fig. 4**). Among the results shown in **Fig. 4a** and **Supplementary Fig. 4**, *CCP2*, *CCP1*, *CAH3*, *BST1* and *LCIA* were least affected by acetate in the WT background, indicating that the level of acetate-derived CO_2 was not sufficient to strongly inhibit expression of these genes (5% CO_2 had a much more pronounced effect). These findings suggest that expression of the CCM genes is differentially sensitive to CO_2 levels.

CIA5 has been shown to regulate accumulation of transcripts from both the CCM genes and *LHCSR3* when *Chlamydomonas* cells are shifted from high to low CO_2 at a constant, moderate light intensity of 100 µmol photons m^{-2} s^{-1} [27,28]. However, the role of CIA5 in acclimation to HL stress has not been analysed. To examine the photoprotection capacity of the *cia5* mutant, LL, air sparged WT and *cia5* cells were shifted to HL and qE effectors gene expression and protein levels were monitored. Remarkably, a lack of *CIA5* resulted in much lower accumulation of *LHCSR3* mRNA than in WT cells (**Fig. 4b)** and although higher transcript levels accumulated when mutant cells were shifted from LL to HL, the level barely exceeded that of WT cells maintained in LL. As a result, no LHCSR3 protein was detected in the mutant in either LL or HL **(Fig. 4c**). The *cia5* mutant appeared to accumulate slightly more *LHCSR1* mRNA in both LL and HL (~2 fold), although there was no difference in the level of the mRNA in the mutant and complemented cells (**Fig. 4b**). Importantly, the LHCSR1 protein accumulated to high levels in the mutant under both LL (conditions in which no protein is apparent in the WT) and HL conditions; this phenotype was fully reversed by ectopic expression of the WT *CIA5* gene (**Fig. 4c**). This result suggests that CIA5 acts as a suppressor of LHCSR1 translation (and/or possibly decreases protein stability) in both LL and HL. These results also suggest that accumulation of LHCSR1 protein occurs through a compensatory, CIA5-controlled posttranscriptional mechanism that provides photoprotection under conditions in which the cells have almost no LHCSR3 protein (compare LHCSR1 and LHCSR3 immunoblots in **Fig. 4b**). Finally, PSBS showed little CIA5 dependent control at the mRNA level (**Fig. 4b**); we were unable to immunologically detect the protein.

To evaluate the impact of the different expression profiles of the photoprotective proteins on the photoprotection capacity of *cia5* mutant, we measured qE levels and found that the *cia5* mutant developed lower qE as compared to WT and (**Fig. 4d** and **Supplementary Fig. 5**)**.** Yet, the qE levels in *cia5* were unexpectedly high considering the absence of LHCSR3 protein (**Fig. 4c**), which can be explained by overaccumulation of LHCSR1 in this mutant (**Fig. 4c)**. All *cia5*-related phenotypes (*LHCSR3* mRNA level, LHCSR3 and LHCSR1 protein accumulation and qE) were fully restored in the complemented *cia5-C* strain (**Fig. 4b-d** and **Supplementary Fig. 5)**. Together, our results demonstrate a key role of CIA5 in the regulation of photoprotection, activating *LHCSR3* and to a lesser extent *PSBS* transcription and suppressing LHCSR1 protein accumulation.

We also quantified accumulation of mRNAs of *CAH1* and *LCIA*, previously described to be strongly dependent on CIA5 [28,39]. The transcripts of all three genes strongly accumulated in WT and *cia5-C* upon the shift from LL to HL (**Fig. 4b**), confirming our findings showing that exposure to HL triggers low CO_2 responses (**Fig. 4a** and **Supplementary Fig. 4)**. As expected, *cia5* mutant cells failed to activate any of those genes in HL while their activation was fully restored in the complemented *cia5-C* strain (**Fig. 4b**).

Interestingly, while CCM gene expression could not be induced in the *cia5* mutant either in LL or HL, this was not the case for the photoprotection-related genes which were activated in the *cia5* mutant when cells were shifted from LL to HL (**Fig. 4b**), although to a much smaller extent than in the WT cells. This indicates that besides CO_2, light is also required to regulate photoprotection, but not CCM-related gene expression.

Intracellular CO_2 levels regulate photoprotective and CCM gene expression in the absence of light

To de-convolute the light and CO_2 signals regulating *LHCSR3*, we exposed the cells to different light intensities (10, 150, and 300 µmol photons m^{-2} s^{-1}) and CO_2 concentrations (0, 0.04, and 5 %) (**Supplementary Fig. 6**). High CO_2 levels completely abolished accumulation of LHCSR3 protein at all light intensities, in accord with the results of **Fig. 1b** and **d**, while near complete elimination of CO_2 from the gas being used to sparge the cultures led to very high accumulation LHCSR3 protein at 150 µmol photons m^{-2} s^{-1}; under these very low CO_2 ($VLCO_2$) conditions, LHCSR3 protein was detectable even at the very low light intensity of 10 µmol photons m^{-2} s^{-1} **(Supplementary Fig. 6)**, as previously demonstrated [6].

Prompted by this result, we tested whether changes in CO_2 levels could activate transcription of *LHCSR3* in complete darkness. Air-bubbled cells were shifted to bubbling with $VLCO_2$ (air passed through soda lime) in complete darkness and the levels of *LHCSR3* mRNA and protein were assayed. To our surprise, we observed that despite the absence of light, a drop in CO_2 availability was sufficient to trigger *LHCSR3* mRNA accumulation by ca. 700-fold (**Fig. 5a**), which was reflected by a 3-fold change in the accumulation of the protein (**Fig 5b** and **c**; compare WT air with WT $VLCO_2$). In addition, when HL was superimposed on very low CO_2-air conditions, which is expected to result in an even greater reduction in the intracellular CO_2 concentration, the levels of *LHCSR3* mRNA and protein further increased, reaching levels of ~4500 fold (mRNA) and 21 fold (protein) compared to air dark conditions (**Fig. 5a-c**). Interestingly, this light-independent regulation of mRNA accumulation was under the control of CIA5 as the *cia5* mutant showed almost abolished accumulation of *LHCSR3* transcripts in the dark when shifted from air to very low CO_2 air (ca. three orders of magnitude less than in WT; **Fig. 5a**). We also observed a significant but smaller decrease of *LHCSR3* transcript accumulation when *cia5* cells were shifted from dark-air to HL-$VLCO_2$ (9 fold lower compared to the WT; **Fig. 5a**). This CIA5-independent regulation of mRNA in the presence of light could account for the contribution of light signaling in *LHCSR3* gene expression, possibly via phototropin [10]. Independently of the extent of the impact of the lack of CIA5 on *LHCSR3* transcript accumulation, the *cia5* mutant did not accumulate significant amounts of LHCSR3 protein under any of the conditions tested (**Fig. 5b**), as in the case of LL to HL experiments (**Fig. 4c**). A full reversal of these phenotypes (gene expression and protein levels) was observed in the *cia5-C* strain (**Fig. 5a** and **b**).

The *LHCSR1* transcripts exhibited generally small differences in accumulation (levels that remained very low) when shifted from dark air to dark $VLCO_2$ conditions; the observed small changes did not appear to be *cia5* dependent (Supplementary **Fig. 7a**), suggesting that CIA5 has no or little (potentially indirect) impact on accumulation of *LHCSR1* transcripts, as already shown by our previous results (**Fig. 4b**). However, LHCSR1 protein over-accumulated in the *cia5* mutant under all conditions tested, although the WT phenotype was only partially restored in *cia5*-C (Supplementary **Fig. 7b**). These results confirm our previous finding that CIA5 impacts the LHCSR1 level by post-transcriptional processes (**Fig. 4b** and **c**). *PSBS* mRNA accumulation did not depend on CIA5 during the shift from dark air to dark $VLCO_2$. Yet, both PSBS RNA and protein accumulation were reduced by ~50% in *cia5* cells shifted from dark air to HL-$VLCO_2$ (Supplementary **Fig. 7a** and **b**), indicating that CIA5 may participate in this regulation, either directly or indirectly. A previous report noted that PSBS protein accumulation was responsive to CO_2 abundance, with its accumulation reaching maximum levels under low CO_2 and HL conditions [6].

We also tested if CCM-related genes could be activated in complete darkness by shifting the cultures from sparging with air to $VLCO_2$. As shown for the CCM-related genes tested (**Fig. 5a** and **Supplementary Fig. 7a**), high levels of their transcripts were observed in the dark when the cells experienced $VLCO_2$ conditions (compare "dark air" with "dark $VLCO_2$"). Light seemed not to play

an important role in the case this activation; the combination of HL and $VLCO_2$ conditions, either elicited very small (less than two-fold) or no additional increase (compare "HL $VLCO_2$" to "dark $VLCO_2$") in their level of the mRNA accumulation (**Fig. 5a** and **Supplementary Fig. 7a**). As expected CIA5 was critical for expression of the CCM genes under all conditions tested **(Fig. 5a** and **Supplementary Fig. 7a**), confirming its well-established regulatory role for CCM gene expression; for example see [27].

Our finding that *LHCSR3* is regulated by light-independent CO_2 availability has guided us in revising the way in which we view the impact of photosynthetic electron flow on LHCSR3 accumulation; i.e. inhibition of LHCSR3 accumulation in photosynthetic mutants or WT cells treated with photosynthetic inhibitors [10,11]. We propose that photosynthetic electron flow facilitates CO_2 fixation, draws down the intracellular CO_2 concentration, thus relieving inhibition of *LHCSR3* transcription. This hypothesis is in accord with the finding that there is a marked increase of CO_2 in cultures treated with DCMU, an inhibitor of photosystem II, measured either as dissolved CO_2 in the culture medium [40] or as CO_2 in the air stream coming out of the headspace of the column bioreactor with a CO_2 gas detector (**Fig. 5d**). We analyzed the impact of DCMU on accumulation of mRNA from the *LHCSR3* and two CCM genes in WT cultures shaken without or with $VLCO_2$ sparging. In accord with previous reports [10,41], DCMU completely blocked the HL elicited accumulation of *LHCSR3* mRNA; the level of mRNA diminished to about ~10% of the initial LL and 0.1% of the HL levels (**Fig. 5e**), which most likely reflects degradation of the transcripts following inactivation of the gene after the addition of DCMU. Previous work has shown that *LHCSR3* transcripts are rapidly lost once the gene becomes inactive [10] which has also been observed for the *CAH4* transcript [42]. Interestingly, a large part of the DCMU elicited inhibition was relieved when the cultures were sparged with $VLCO_2$ air (**Fig. 5e**), which would result in maintenance of a continuous $VLCO_2$ concentration in the cultures and supports that idea that light primarily impacts *LHCSR3* transcript levels by altering CO_2 consumption and the intracellular (and/or extracellular) CO_2 concentration. In contrast to *LHCSR3*, sparging with $VLCO_2$ only partly relieved the suppression of transcript accumulation for the CCM genes in the presence of DCMU (**Fig. 5e**). This difference may reflect the fact that CCM gene expression is solely regulated by CO_2 via CIA5 (**Fig. 5a**) and that sparging with $VLCO_2$ in the presence of DCMU does not reduce the CO_2 levels enough to attain full gene activation; on the other hand, light does contribute to *LHCSR3* mRNA accumulation as seen for the *cia5* mutant in **Fig. 5a**, likely through the action of phototropin [10]. It is also possible that longer incubation time with $VLCO_2$ would have relieved a larger part of the DCMU-elicited inhibition of CCM genes (**Fig. 5e**) as implied by the slow kinetics of *CAH4/5* mRNA accumulation when cells are shifted from 5% CO_2 to air [42].

Discussion

In this work, we presented findings that advance our understanding of the integration between CO_2- and light-dependent signaling in *Chlamydomonas*. Our data demonstrate that the intracellular levels of CO_2, defined by the equilibrium between CO_2 fixation in chloroplasts and the generation of CO_2 by mitochondrial metabolism (e.g. acetate assimilation), is a key determinant in the regulation of gene expression controlling two major processes of photosynthetic organisms: CCM and photoprotection (**Fig. 6**).

LHCSR3 is widely accepted as the central qE effector protein in *Chlamydomonas* cells challenged with high levels of visible light [5,43]. It was recently shown that cells grown in the presence of acetate do not accumulate LHCSR3 protein [25], yet there was little understanding of the molecular mechanism of this inhibition. We propose that the inhibition of LHCSR3 by acetate occurs at the transcription level (**Fig. 1a** and **c**). The use of *icl* and *dum11* mutants, both impaired in acetate metabolism (**Fig. 1**), coupled with time resolved analyses of gene expression for *LHCSR3* and *RHP1*, a high CO_2 responsive gene (**Fig. 2**), were instrumental in demonstrating that acetate impacted *LHCSR3* expression levels only if it was metabolized, leading to increased levels of CO_2. This finding was supported by our metabolic modeling approach (**Supplementary Fig. 1, Supplementary Tables 1 and 2, Supplementary Data 1**) that provided an unbiased view of changes in the activity of metabolic reactions directly involved in acetate metabolism and its consequences on related pathways. Overall, the modeling allowed us to identify a combination of conditions in both WT and mutant strains that supported the hypothesis that larger intracellular CO_2 levels result from acetate metabolism. The acetate derived respiratory-produced CO_2 is assimilated in chloroplasts through photosynthetic CO_2 fixation, as evidenced by the higher photosynthetic performance (probed as rETR) of acetate-supplemented cultures of WT and *icl-C* but not of *icl* (**Supplementary Fig. 2a**). In addition to the impact of acetate on *LHCSR3* expression, cells grown on acetate do not activate CCM or properly express CCM related genes [23,42,44], and their chloroplasts failed to concentrate inorganic carbon [24]. In our study, the CCM genes exhibited a similar expression profile as *LHCSR3*, namely, they were suppressed by acetate in WT but not in the *icl* mutant (**Fig. 4a** and **Supplementary Fig. 4**). These results validate earlier predictions that that CO_2 released by the metabolism of acetate mimics high-CO_2 conditions and inhibits CCM [24,42,45].

Not only acetate, but sparging with 5% CO_2 also inhibited *LHCSR3* expression (**Fig. 1**). Interestingly, our kinetic analyses of changes in levels of transcripts and proteins encoded by the photoprotective genes revealed significant differences among the responses of *LHCSR3*, *LHCSR1* and *PSBS* to CO_2. Increased CO_2 levels were found to dramatically repress *LHCSR3* mRNA accumulation, in agreement with previously published works [27,28], but had little impact on accumulation of *LHCSR1* and *PSBS* transcripts (**Fig. 3**). While a good correlation between mRNA and protein levels was observed for LHCSR3, this was not the case for LHCSR1; high CO_2 sustained high levels of LHCSR1 protein (**Fig. 3**) suggesting that CO_2 either enhances translation of and/or stabilizes LHCSR1. The finding that *LHCSR3* responds to changes in CO_2 availability was originally reported by Miura and colleagues [28] and later validated by genome-wide transcript analyses [27,46,47]. Here, we show that exposure of LL maintained cells to HL decreases intracellular CO_2 levels, as suggested by *RHP1* repression (**Fig. 2e**), and that this decrease impacts the expression of both photoprotection- and CCM-related genes (**Fig. 4a** and **Supplementary Fig. 4**). Our results provide then an explanation for the previously observed accumulation of CCM proteins under HL conditions [37,48]. The close interconnection of photoprotection, CCM and CO_2 is further substantiated by the finding that CIA5, the regulator of the CCM-associated genes, also exerts control over *LHCSR3* and to a much lesser extent over *PSBS* mRNA levels (**Fig. 4b**), as well as over LHCSR1 protein levels; for LHCSR1, CIA5 can repress post-transcriptional processes either directly or indirectly (protein translation or stability) (**Fig. 4c**). *CIA5* mRNA and protein have been found to be similarly expressed under high and low CO_2 conditions, suggesting that

posttranslational modifications (either directly on CIA5 or on an interacting protein) regulate its activity during transitions between high and low CO_2 concentrations [16,17]. High CO_2 levels inactivate CIA5. Therefore, high CO_2-acclimated WT cells would not be subjected to CIA5 control, and the finding that *cia5* over-accumulates LHCSR1 protein (**Fig. 4c**) is in good agreement with the increase of LHCSR1 protein levels observed in WT cells in the presence of 5% CO_2 (**Fig. 3b**). CIA5 has been known as the master regulator of CCM [28] because it controls most CCM-related genes. Yet, as our data suggest, its regulatory function also encompasses genes involved in photoprotection (**Fig. 4** and **6**).

To better understand the role of CO_2 in regulating photoprotection and its integration with light, we designed experiments to separate the effects of the two signals (**Fig. 5** and **6**); we reduced the concentration of CO_2 in the microalgae medium by sparging it with $VLCO_2$, and worked in complete darkness. The transition from air-CO_2 to $VLCO_2$ levels in the dark strongly increased *LHCSR3* transcript levels (**Fig. 5**), a very surprising result as *LHCSR3* mRNA accumulation was considered to be strictly light-dependent. Moreover, we observed that while dark induction of *LHCSR3* under CO_2-depletion was fully CIA5 dependent, light could still strongly impact expression of all photoprotective genes in the *cia5* mutant, which was not the case for CCM gene expression which was completely abolished in the light or dark in the absence of CIA5 (**Fig. 5**). This impact of light on *LHCSR3* expression may be the consequence of photoperception (e.g. phototropin) [10], but also the generation of light-dependent signals such as reactive oxygen species [49]. This CIA5-independent regulation would explain *LHCSR3* induction in high CO_2-acclimated WT cells (cells in which CIA5 is not functional) when transitioning from LL to HL (**Fig. 1a**), which was not observed for CCM genes when tested under the same conditions (**Fig. 4a** and **Supplementary Fig. 4**). CO_2 and CIA5 appear to be of paramount importance in signal integration and transduction, regulating expression of both photoprotection and CCM genes. For instance, CO_2 represses the UV-B elicited and UVR8-mediated expression of *LHCSR3* and CIA5 is crucial for this expression [49]. Moreover, our results have shown that high CO_2 levels or the absence of CIA5 have a severe impact on *LHCSR3* gene expression and, although HL can still induce *LHCSR3* transcription, no protein is detected (**Fig. 1, 4** and **5**).

Our data demonstrate that most of the light impact on *LHCSR3* expression is indirect and reflects changes in intracellular CO_2 levels. This notion explains for instance why a shift from TAP to HSM under LL leads to significant LHCSR3 protein accumulation[48]; the removal of acetate present in the TAP medium lead to a sudden drop in CO_2 (produced via acetate catabolism) and accumulation of *LHCSR3* mRNA. This was recently reported by Redekop and colleagues; *LHCSR3* mRNA accumulated in the dark, in a CIA5-dependent manner, upon changing the medium from TAP to TP [49], which is congruent with the results of this study. On the other hand, since the discovery that active photosynthetic electron flow is required for the LHCSR3 accumulation [11], and also for CCM activation and CCM gene expression [50], the nature of the signal linking chloroplast activity with nuclear expression of LHCSR3 has remained elusive. We propose that CO_2, either directly or indirectly via a CO_2-dependent metabolic change, is the missing link between photosynthetic electron flow and the transcriptional regulation of *LHCSR3* and the CCM genes (**Fig. 5d** and **e)**, as active photosynthesis draws down cellular CO_2 levels. Accordingly, blocking photosynthesis with DCMU leads to the accumulation of CO_2 (**Fig. 5d**) which causes *LHCSR3* repression, while sparging DCMU-treated cells with $VLCO_2$ almost fully derepresses *LHCSR3* (and partially CCM) expression (**Fig. 5e**). DCMU also upregulates genes of the leucine degradation pathway [51] leading to the generation of acetoacetate and acetyl-CoA, whose oxidation would lead to CO_2 production. Whether leucine itself has a regulatory role or CO_2 is the key regulator deserves further investigation. It is tempting to propose that CO_2 could be considered as a retrograde signal for remote control of nuclear gene expression, integrating both mitochondrial and chloroplastic metabolic activities.

Dark induction of CCM genes (*CAH1, CAH3, CAH4, CAH6, LCIB*) has been shown to occur in synchronized (12 h light / 12 h dark) *Chlamydomonas* cultures [42,52-54]. In non-synchronous cultures, only CAH1 protein accumulation has been reported to take place in the dark [55,56]. Here, we provide a more comprehensive view of the dependence of CCM gene activation on the light availability; CCM genes were strongly activated in non-synchronous culture by sparging the cell cultures with $VLCO_2$ in the dark (**Fig. 5a**). This activation was CIA5-dependent and not further enhanced (or to a very small extent) by superimposing HL, which would further draw down the intracellular CO_2 levels. This indicates that most, if not all available CO_2 was depleted in the soda-lime-treated air used for establishing $VLCO_2$. This abrupt change in CO_2 levels applied in the dark may be viewed as a condition only encountered in the laboratory. Yet, in certain ecological niches, such as soil or catchments with elevated levels of organic matter [38], *Chlamydomonas* would encounter changes in the levels of CO_2 that would be dependent on the microbial composition and the ratio between respiration and photosynthesis. The way in which *Chlamydomonas* senses CO_2 is not clear. Our data, i.e. accumulation of *LHCSR3* and CCM genes in the dark, exclude the possibility that a metabolite produced by photorespiration plays a major signalling role, as previously proposed [57]. CO_2 itself might also serve as the metabolite being recognized by a putative sensor that could be controlled by carbamylation, a CO_2-mediated post-translational modification that regulates, among others, the activation of Rubisco [58]. Furthermore, the large number of adenosine and guanylyl cyclases in *Chlamydomonas* [59] suggests that cyclic nucleotides play an important role in this alga; they have been shown to be involved in mating [60], regulation of flagellar beating and phototaxis [61-63], in regulating inorganic nitrogen assimilation [64] and in restoring LHCSR3 accumulation in the absence of phototropin [10]. Cyclases have been shown to act as CO_2 sensors (as bicarbonate) in mammalian cells (*75*) making it plausible that they can also serve as sensors in *Chlamydomonas*. As cyclic nucleotide signalling and calcium are tightly linked [65], we anticipate an important role for calcium in CO_2 sensing; calcium signalling has already been shown to be involved in the regulation of both *LHCSR3* and CCM genes [11,66].

Overall, our work shows (**Fig. 6**) that the intracellular CO_2 level is the main factor in regulating CCM genes and *LHCSR3* in *Chlamydomonas*. Exposure to HL increases the CO_2 fixation rate which causes a drop in intracellular CO_2 which, in turn, actives both photoprotection- and CCM-related genes. Depletion of CO_2 in complete darkness can also elicit elevated expression of *LHCSR3* and the CCM genes. High CO_2 levels, either generated through enhanced respiratory activity or impaired photosynthetic electron transport, repress *LHCSR3* and CCM genes while at the same time stabilizing the LHCSR1 protein. Furthermore, our data shows that CIA5 is a central regulator of photoprotection, exerting control over *LHCSR3* and to a lesser extent over *PSBS* mRNA levels, while repressing LHCSR1 protein accumulation. The CIA5-independent light-dependent induction of photoprotective genes possibly involves phototropin, as previous shown [10], but may also involve retrograde signals such as reactive species [49,67]. Our findings also highlight the need to develop an integrated approach that examines the role of CO_2 and light, with respect to CO_2 fixation, photoreceptors, and redox conditions on the regulation of photoprotection and to consider photoprotection in a broader context that includes various processes involved in managing the use and consequences of absorbing excess excitation.

Materials and methods

Chemicals

DCMU (3-(3,4-dichlorophenyl)-1,1-dimethylurea) was purchased from Sigma. Stock solutions of DCMU were prepared in ethanol (40 mM).

Strains and conditions

C. reinhardtii strains were grown under 20 µmol photons m^{-2} s^{-1} in Tris-acetate-phosphate (TAP) media [68] at 23 °C in Erlenmeyer flasks shaken at 125 rpm. For all experiments cells were transferred to Sueoka's high salt medium [69] supplemented when needed with 10 mM sodium acetate, at 2 million cells mL^{-1} in 80 mL capacity columns, unless otherwise stated, sparged with air, air enriched with 5% CO_2, or very low CO_2 air ($VLCO_2$; generated by passing the air through soda lime) and exposed to light intensities as described in the text and figure legends. *C. reinhardtii* strain 137c mt+ was used as WT. The *icl* (defective in *ICL1*; gene ID: Cre06.g282800), *dum11* (defective in defective in ubiquinol cytochrome c oxidoreductase of the respiratory complex III; geneID: CreMt.g000300) *and cia5* (defective in *CIA5*, aka CCM1; geneID: Cre02.g096300; *Chlamydomonas* Resource Centre strain CC-2702) mutants were previously generated [15,21,29]. For the complementation of *cia5*, a 3.5-kbp genomic DNA fragment from CC-125 containing *CIA5* coding region was amplified by PCR using Platinum™ SuperFi™ DNA Polymerase (Thermo Fisher Scientific) and primers gib-cia5-fw and gib-cia5-rev (**Supplementary Table 3**), gel purified and cloned into pLM005 [70] by Gibson assembly [71] for expression under control of the *PSAD* promoter. Junctions and insertion were sequenced and constructs were linearized by EcoRV before transformation into *cia5*. Eleven ng/kb of linearized plasmid [70] mixed with 400 µL of 1.0 x10^7 cells mL^{-1} were electroporated in a volume of 120 mL in a 2-mm-gap electro cuvette using a NEPA21 square-pulse electroporator (NEPAGENE, Japan). The electroporation parameters were set as follows: Poring Pulse (300V; 8 ms length; 50 ms interval; one pulse; 40% decay rate; + Polarity), Transfer Pluse (20V; 50 ms length; 50 ms interval; five pulses; 40% decay rate; +/- Polarity). Transformants were selected onto solid agar plates containing 10 µg/ml paromomycin and screened for fluorescence by using a Tecan fluorescence microplate reader (Tecan Group Ltd., Switzerland). Parameters used were as follows: YFP (excitation 515/12 nm and emission 550/12 nm) and chlorophyll (excitation 440/9 nm and 680/20 nm). Transformants showing high YFP/chlorophyll value were further analyzed by immunoblotting using anti-FLAG antibody (**Fig. S7**). Among the transformants analyzed the *cia5-C-a1* (*cia5-C* throughout the text) was retained for further analyses in the present study. Unless otherwise stated, LL conditions corresponded to 20 µmol photons m^{-2} s^{-1} while HL conditions corresponded to 600 µmol photons m^{-2} s^{-1} of white light (Neptune L.E.D., France; see **Supplementary Fig. 9** for light spectrum). All experiments were repeated three times to verify their reproducibility, unless otherwise stated.

Fluorescence-based measurements

Fluorescence-based photosynthetic parameters were measured with a a pulse modulated amplitude fluorimeter (MAXI-IMAGING-PAM, HeinzWaltz GmbH, Germany). Prior to the onset of the measurements, cells were acclimated to darkness for 15 min. Chlorophyll fluorescence was recorded under different intensities f actinic light; starting with measurements in the dark (indicated as D below the x-axis of the graphs), followed by measurements at 21 µmol photons m^{-2} s^{-1} (indicated as L1 below the x-axis of the graphs) and 336 µmol photons m^{-2} s^{-1} (indicated as L2 below the x-axis of the graphs) and finishing with measurements of fluorescence relaxation in the dark. The calculations of the different photosynthetic parameter was performed based on [72] as follows: The relative photosynthetic electron transfer rate (rETR) was calculated as ($Fm' - F$)/Fm' × I; F and Fm' are the fluorescence yield in steady state light and after a saturating pulse in the actinic light, respectively; ; I is the light irradiance in µmol photons m^{-2} s^{-1}; NPQ was calculated

as (Fm − Fm′)/Fm′; Fm is the maximal fluorescence yield in dark-adapted cells ; the effective photochemical quantum yield of photosystem II was calculated as Y(II) = (Fm'-F)/Fm'; qE was estimated as the fraction of NPQ that is rapidly inducible in the light and reversible in the dark.

mRNA quantification

Total RNA was extracted using the RNeasy Mini Kit (Qiagen) and treated with the RNase-Free DNase Set (Qiagen). 1 µg total RNA was reverse transcribed with oligo dT using Sensifast cDNA Synthesis kit (Meridian Bioscience, USA). qPCR reactions were performed and quantitated in a Bio-Rad CFX96 system using SsoAdvanced Universal SYBR Green Supermix (BioRad). The primers (0.3 µM) used for qPCR are listed in **Supplementary Table 3**. A gene encoding G protein subunit-like protein (GBLP)[73] was used as the endogenous control , and relative expression values relative to *GBLP* were calculated from three biological replicates, each of which contained three technical replicates.

CO_2 measurements

CO_2 concentration was measured in the air stream coming out of the headspace of a HSM or culture containing column using the CO_2 Probe GMP251 connected to the MI70 data logger from Vaisala (Vantaa, Finland).

Immunoblotting

Protein samples of whole cell extracts (0.5 µg chlorophyll or 10 µg protein) were loaded on 4-20% SDS-PAGE gels (Mini-PROTEAN TGX Precast Protein Gels, Bio-Rad) and blotted onto nitrocellulose membranes. Antisera against LHCSR1 (AS14 2819), LHCSR3 (AS14 2766), ATPB (AS05 085), CAH4/5 (AS11 1737) were from Agrisera (Vännäs, Sweden); previously described was antisera against *C. reinhardtii* PSBS [6]. ATPB was used as a loading control. An anti-rabbit horseradish peroxidase–conjugated antiserum was used for detection. The blots were developed with ECL detection reagent, and images of the blots were obtained using a CCD imager (ChemiDoc MP System, Bio-Rad). For the densitometric quantification, data were normalized with ATPB.

Statistical analyses

All statistical tests were performed using the computing environment Prism 9 (Graphpad Software, LLC), with a significance level of 0.05. In order to conform mRNA accumulation data to the distributional assumptions of ANOVA, i.e. the residuals should be normally distributed and variances should be equal among groups, Two-Way Analysis of Variance were computed with log-transformed data Y=logX where X is mRNA accumulation [74].

References

1. Li, Z., Wakao, S., Fischer, B. B. & Niyogi, K. K. Sensing and responding to excess light. *Annu. Rev. Plant Biol.* **60,** 239–260 (2009).
2. Bennett, D. I. G. *et al.* Models and mechanisms of the rapidly reversible regulation of photosynthetic light harvesting. *Open Biol* **9,** 190043 (2019).
3. Alboresi, A., Gerotto, C., Giacometti, G. M., Bassi, R. & Morosinotto, T. Physcomitrella patens mutants affected on heat dissipation clarify the evolution of photoprotection mechanisms upon land colonization. *Proc. Natl. Acad. Sci. U.S.A.* **107,** 11128–11133 (2010).
4. Niyogi, K. K. & Truong, T. B. Evolution of flexible non-photochemical quenching mechanisms that regulate light harvesting in oxygenic photosynthesis. *Curr. Opin. Plant Biol.* **16,** 307–314 (2013).
5. Peers, G. *et al.* An ancient light-harvesting protein is critical for the regulation of algal photosynthesis. *Nature* **462,** 518–521 (2009).
6. Correa-Galvis, V. *et al.* Photosystem II Subunit PsbS Is Involved in the Induction of LHCSR Protein-dependent Energy Dissipation in Chlamydomonas reinhardtii. *J. Biol. Chem.* **291,** 17478–17487 (2016).
7. Tibiletti, T., Auroy, P., Peltier, G. & Caffarri, S. Chlamydomonas reinhardtii PsbS Protein Is Functional and Accumulates Rapidly and Transiently under High Light. *Plant Physiol.* **171,** 2717–2730 (2016).
8. Allorent, G. *et al.* UV-B photoreceptor-mediated protection of the photosynthetic machinery in Chlamydomonas reinhardtii. *Proc. Natl. Acad. Sci. U.S.A.* **113,** 14864–14869 (2016).
9. Dinc, E. *et al.* LHCSR1 induces a fast and reversible pH-dependent fluorescence quenching in LHCII in Chlamydomonas reinhardtii cells. *Proc. Natl. Acad. Sci. U.S.A.* **113,** 7673–7678 (2016).
10. Petroutsos, D. *et al.* A blue-light photoreceptor mediates the feedback regulation of photosynthesis. *Nature* **537,** 563–566 (2016).
11. Petroutsos, D. *et al.* The chloroplast calcium sensor CAS is required for photoacclimation in *Chlamydomonas reinhardtii*. *Plant Cell* **23,** 2950–2963 (2011).
12. Tokutsu, R., Fujimura-Kamada, K., Matsuo, T., Yamasaki, T. & Minagawa, J. The CONSTANS flowering complex controls the protective response of photosynthesis in the green alga Chlamydomonas. *Nat Comms* **10,** 655–10 (2019).
13. Gabilly, S. T. *et al.* Regulation of photoprotection gene expression in Chlamydomonas by a putative E3 ubiquitin ligase complex and a homolog of CONSTANS. *Proc. Natl. Acad. Sci. U.S.A.* **116,** 17556–17562 (2019).
14. Maberly, S. C. & Gontero, B. Ecological imperatives for aquatic CO2-concentrating mechanisms. *J. Exp. Bot.* **68,** 3797–3814 (2017).
15. Moroney, J. V. *et al.* Isolation and Characterization of a Mutant of Chlamydomonas reinhardtii Deficient in the CO2 Concentrating Mechanism. *Plant Physiol.* **89,** 897–903 (1989).
16. Fukuzawa, H. *et al.* Ccm1, a regulatory gene controlling the induction of a carbon-concentrating mechanism in Chlamydomonas reinhardtii by sensing CO2 availability. *Proc. Natl. Acad. Sci. U.S.A.* **98,** 5347–5352 (2001).
17. Xiang, Y., Zhang, J. & Weeks, D. P. The Cia5 gene controls formation of the carbon concentrating mechanism in Chlamydomonas reinhardtii. *Proc. Natl. Acad. Sci. U.S.A.* **98,** 5341–5346 (2001).
18. Harris, E. H. Chlamydomonas as a Model Organism. *Annu. Rev. Plant. Physiol.* (2001). doi:10.1146/annurev.arplant.52.1.363

19. Wolfe, A. J. The acetate switch. *Microbiol. Mol. Biol. Rev.* **69,** 12–50 (2005).
20. Kornberg, H. L. & Krebs, H. A. *Synthesis of cell constituents from C2-units by a modified tricarboxylic acid cycle. Nature* **179,** 988–991 (Nature, 1957).
21. Plancke, C. *et al.* Lack of isocitrate lyase in Chlamydomonas leads to changes in carbon metabolism and in the response to oxidative stress under mixotrophic growth. *Plant J.* **77,** 404–417 (2014).
22. Salinas, T., Larosa, V., Cardol, P., Marechal-Drouard, L. & Remacle, C. Respiratory-deficient mutants of the unicellular green alga Chlamydomonas: A review. *Biochimie* (2013). doi:10.1016/j.biochi.2013.10.006
23. Fett, J. P. & Coleman, J. R. Regulation of periplasmic carbonic anhydrase expression in Chlamydomonas reinhardtii by acetate and pH. *Plant Physiol.* **106,** 103–108 (1994).
24. Moroney, J. V., Kitayama, M., Togasaki, R. K. & Tolbert, N. E. Evidence for Inorganic Carbon Transport by Intact Chloroplasts of Chlamydomonas reinhardtii. *Plant Physiol.* **83,** 460–463 (1987).
25. Polukhina, I., Fristedt, R., Dinc, E., Cardol, P. & Croce, R. Carbon supply and photoacclimation crosstalk in the green alga Chlamydomonas reinhardtii. *Plant Physiol.* 1494–1505 (2016). doi:10.1104/pp.16.01310
26. Roach, T., Sedoud, A. & Krieger-Liszkay, A. Acetate in mixotrophic growth medium affects photosystem II in Chlamydomonas reinhardtii and protects against photoinhibition. *Biochim. Biophys. Acta* **1827,** 1183–1190 (2013).
27. Fang, W. *et al.* Transcriptome-wide changes in Chlamydomonas reinhardtii gene expression regulated by carbon dioxide and the CO2-concentrating mechanism regulator CIA5/CCM1. *Plant Cell* **24,** 1876–1893 (2012).
28. Miura, K. *et al.* Expression profiling-based identification of CO2-responsive genes regulated by CCM1 controlling a carbon-concentrating mechanism in Chlamydomonas reinhardtii. *Plant Physiol.* **135,** 1595–1607 (2004).
29. Colin, M. *et al.* Mutations affecting the mitochondrial genes encoding the cytochrome oxidase subunit I and apocytochrome b of Chlamydomonas reinhardtii. *Molec. Gen. Genet.* **249,** 179–184 (1995).
30. Nawrocki, W. J., Liu, X. & Croce, R. Chlamydomonas reinhardtii Exhibits De Facto Constitutive NPQ Capacity in Physiologically Relevant Conditions. *Plant Physiol.* **182,** 472–479 (2020).
31. Hanawa, Y., Watanabe, M., Karatsu, Y., Fukuzawa, H. & Shiraiwa, Y. Induction of a high-CO2-inducible, periplasmic protein, H43, and its application as a high-CO2-responsive marker for study of the high-CO2-sensing mechanism in Chlamydomonas reinhardtii. *Plant Cell Physiol.* **48,** 299–309 (2007).
32. Soupene, E. *et al.* Rhesus expression in a green alga is regulated by CO(2). *Proc. Natl. Acad. Sci. U.S.A.* **99,** 7769–7773 (2002).
33. Ballottari, M. *et al.* Identification of pH-sensing Sites in the Light Harvesting Complex Stress-related 3 Protein Essential for Triggering Non-photochemical Quenching in Chlamydomonas reinhardtii. *J. Biol. Chem.* **291,** 7334–7346 (2016).
34. Burlacot, A. *et al.* Alternative electron pathways of photosynthesis drive the algal CO2 concentrating mechanism. *bioRxiv* 2021.02.25.432959 (2021). doi:10.1101/2021.02.25.432959
35. Mukherjee, A. *et al.* Thylakoid localized bestrophin-like proteins are essential for the CO2 concentrating mechanism of Chlamydomonas reinhardtii. *Proc. Natl. Acad. Sci. U.S.A.* **116,** 16915–16920 (2019).
36. Aihara, Y., Fujimura-Kamada, K., Yamasaki, T. & Minagawa, J. Algal photoprotection is regulated by the E3 ligase CUL4-DDB1DET1. *Nature Plants* **5,** 34–40 (2019).

37. Scholz, M. *et al.* Light-dependent N-terminal phosphorylation of LHCSR3 and LHCB4 are interlinked in Chlamydomonas reinhardtii. *Plant J.* **99,** 877–894 (2019).
38. Wang, Y., Stessman, D. J. & Spalding, M. H. The CO2 concentrating mechanism and photosynthetic carbon assimilation in limiting CO2 : how Chlamydomonas works against the gradient. *Plant J.* **82,** 429–448 (2015).
39. Yoshioka, S. *et al.* The novel Myb transcription factor LCR1 regulates the CO2-responsive gene Cah1, encoding a periplasmic carbonic anhydrase in Chlamydomonas reinhardtii. *Plant Cell* **16,** 1466–1477 (2004).
40. Hanawa, Y., Watanabe, M., Karatsu, Y., Fukuzawa, H. & Shiraiwa, Y. Induction of a high-CO2-inducible, periplasmic protein, H43, and its application as a high-CO2-responsive marker for study of the high-CO2-sensing mechanism in Chlamydomonas reinhardtii. *Plant Cell Physiol.* **48,** 299–309 (2007).
41. Maruyama, S., Tokutsu, R. & Minagawa, J. Transcriptional regulation of the stress-responsive light harvesting complex genes in *Chlamydomonas reinhardtii*. *Plant Cell Physiol.* **55,** 1304–1310 (2014).
42. Eriksson, M., Villand, P., Gardeström, P. & Samuelsson, G. Induction and Regulation of Expression of a Low-CO2-Induced Mitochondrial Carbonic Anhydrase inChlamydomonas reinhardtii. *Plant Physiol.* **116,** 637–641 (1998).
43. Allorent, G. & Petroutsos, D. Photoreceptor-dependent regulation of photoprotection. *Curr. Opin. Plant Biol.* **37,** 102–108 (2017).
44. Urzica, E. I. *et al.* Systems and trans-system level analysis identifies conserved iron deficiency responses in the plant lineage. *Plant Cell* **24,** 3921–3948 (2012).
45. Fett, J. P. & Coleman, J. R. Regulation of Periplasmic Carbonic Anhydrase Expression in Chlamydomonas reinhardtii by Acetate and pH. *Plant Physiol.* **106,** 103–108 (1994).
46. Brueggeman, A. J. *et al.* Activation of the carbon concentrating mechanism by CO2 deprivation coincides with massive transcriptional restructuring in Chlamydomonas reinhardtii. *Plant Cell* **24,** 1860–1875 (2012).
47. Strenkert, D. *et al.* Multiomics resolution of molecular events during a day in the life of Chlamydomonas. *Proc. Natl. Acad. Sci. U.S.A.* **116,** 2374–2383 (2019).
48. Barth, J. *et al.* The interplay of light and oxygen in the reactive oxygen stress response of Chlamydomonas reinhardtii dissected by quantitative mass spectrometry. *Mol. Cell Proteomics* **13,** 969–989 (2014).
49. Redekop, P. *et al.* Transcriptional regulation of photoprotection in dark-to-light transition-more than just a matter of excess light energy. *Sci Adv* (2022).
50. Spalding, M. H. in *The molecular Biology of Chloroplasts and Mitochondria in Chlamydomonas* (eds. Rochaix, J. D., Goldschmidt-Clermont, M. & Merchant, S. S.) (1998).
51. Hemschemeier, A. *et al.* COPPER RESPONSE REGULATOR1-dependent and -independent responses of the Chlamydomonas reinhardtii transcriptome to dark anoxia. *Plant Cell* **25,** 3186–3211 (2013).
52. Rawat, M. & Moroney, J. V. The Regulation of Carbonic Anhydrase and Ribulose-1,5-Bisphosphate Carboxylase/Oxygenase Activase by Light and CO2 in Chlamydomonas reinhardtii. *Plant Physiol.* **109,** 937–944 (1995).
53. Tirumani, S., Kokkanti, M., Chaudhari, V., Shukla, M. & Rao, B. J. Regulation of CCM genes in Chlamydomonas reinhardtii during conditions of light–dark cycles in synchronous cultures. *Plant Mol. Biol.* **85,** 277–286 (2014).
54. Mitchell, M. C., Meyer, M. T. & Griffiths, H. Dynamics of carbon-concentrating mechanism induction and protein relocalization during the dark-to-light transition in synchronized Chlamydomonas reinhardtii. *Plant Physiol.* **166,** 1073–1082 (2014).

55. Villarejo, A., Reina, G. G. & Ramazanov, Z. Regulation of the low-CO2-inducible polypeptides in Chlamydomonas reinhardtii. *Planta* **199,** 481–485 (1996).
56. Bailly, J. & Coleman, J. R. Effect of CO2 Concentration on Protein Biosynthesis and Carbonic Anhydrase Expression in Chlamydomonas reinhardtii. *Plant Physiol* (1988). doi:10.1104/pp.87.4.833
57. Santhanagopalan, I., Wong, R., Mathur, T. & Griffiths, H. Orchestral manoeuvres in the light: crosstalk needed for regulation of the Chlamydomonas carbon concentration mechanism. *J. Exp. Bot.* **72,** 4604–4624 (2021).
58. Linthwaite, V. L. *et al.* The identification of carbon dioxide mediated protein post-translational modifications. *Nat Comms* **9,** 3092 (2018).
59. Merchant, S. S. *et al.* The Chlamydomonas genome reveals the evolution of key animal and plant functions. *Science* **318,** 245–250 (2007).
60. Hasegawa, E., Hayashi, H., Asakura, S. & Kamiya, R. Stimulation of in vitro motility of Chlamydomonas axonemes by inhibition of cAMP-dependent phosphorylation. *Cell Motil. Cytoskeleton* **8,** 302–311 (1987).
61. Pasquale, S. M. & Goodenough, U. W. Cyclic AMP functions as a primary sexual signal in gametes of Chlamydomonas reinhardtii. *J. Cell Biol.* **105,** 2279–2292 (1987).
62. Gaillard, A. R., Fox, L. A., Rhea, J. M., Craige, B. & Sale, W. S. Disruption of the A-kinase anchoring domain in flagellar radial spoke protein 3 results in unregulated axonemal cAMP-dependent protein kinase activity and abnormal flagellar motility. *Mol. Biol. Cell* **17,** 2626–2635 (2006).
63. Boonyareth, M., Saranak, J., Pinthong, D., Sanvarinda, Y. & Foster, K. W. Roles of cyclic AMP in regulation of phototaxis in *Chlamydomonas reinhardtii*. *Biologia* **64,** 1058–1065 (2009).
64. de Montaigu, A., Sanz-Luque, E., Galván, A. & Fernández, E. A soluble guanylate cyclase mediates negative signaling by ammonium on expression of nitrate reductase in Chlamydomonas. *Plant Cell* **22,** 1532–1548 (2010).
65. Beavo, J. A. & Brunton, L. L. Cyclic nucleotide research -- still expanding after half a century. *Nature* **3,** 710–718 (2002).
66. Wang, L. *et al.* Chloroplast-mediated regulation of CO2-concentrating mechanism by Ca2+-binding protein CAS in the green alga Chlamydomonas reinhardtii. *Proc. Natl. Acad. Sci. U.S.A.* **113,** 12586–12591 (2016).
67. Roach, T., Baur, T., Stöggl, W. & Krieger-Liszkay, A. Chlamydomonas reinhardtii responding to high light: A role for 2-propenal (acrolein). *Physiol Plant* (2017). doi:10.1111/ppl.12567
68. Gorman, D. S. & Levine, R. P. Cytochrome f and plastocyanin: their sequence in the photosynthetic electron transport chain of *Chlamydomonas reinhardii*. *Proc. Natl. Acad. Sci. U.S.A.* **54,** 1665–1669 (1965).
69. Sueoka, N. Mitotic replication of deoxyribonucleic acid in *Chlamydomonas reinhardii*. *Proc. Natl. Acad. Sci. U.S.A.* **46,** 83–91 (1960).
70. Mackinder, L. C. M. *et al.* A repeat protein links Rubisco to form the eukaryotic carbon-concentrating organelle. *Proc. Natl. Acad. Sci. U.S.A.* **113,** 5958–5963 (2016).
71. Gibson, D. G. *et al.* Enzymatic assembly of DNA molecules up to several hundred kilobases. *Nat. Methods* **6,** 343–345 (2009).
72. Genty, B., Briantais, J.-M. & Baker, N. R. The relationship between the quantum yield of photosynthetic electron transport and quenching of chlorophyll fluorescence. *Biochimica et Biophysica Acta (BBA)* **990,** 87–92 (1989).
73. Schloss, J. A. A Chlamydomonas gene encodes a G protein beta subunit-like polypeptide. *Molec. Gen. Genet.* **221,** 443–452 (1990).

74. Schlesselman, J. J. Data Transformation in Two-Way Analysis of Variance. *Journal of the American Statistical Association* (2012). doi:10.1080/01621459.1973.10482435

Acknowledgments

We are grateful to Dr. Konomi Fujimura-Kamada for performing experiments to validate the dark induction of LHCSR3 in the Minagawa lab; to Claire Remacle for sharing the *icl* and *icl-C* strains and Pierre Cardol for the *dum11* strain. We thank Eric Soupene for valuable insights in the RHP1 induction conditions. We thank Dimitra Karageorgou for performing preliminary experiments in the project and Gilles Curien for fruitful discussions on aspects of microalgae metabolism.

Funding:

The authors would like to thank the following agencies for funding: The Human Frontiers Science Program through the funding of the project RGP0046/2018 (DP, GV, YY, ARG, PR, ES-L, ZN, AK); the French National Research Agency in the framework of the Young Investigators program ANR-18-CE20-0006 through the funding of the project MetaboLight (DP, GV, YY); the French National Research Agency through the funding of the Grenoble Alliance for Integrated Structural & Cell Biology GRAL project ANR-17-EURE-0003 (DP, MAR-S, GV, YY); the French National Research Agency in the framework of the Investissements d'Avenir program ANR-15-IDEX-02, through the funding of the "Origin of Life" project of the Univ. Grenoble-Alpes (DP, GV, YY) ; the Prestige Marie-Curie co-financing grant PRESTIGE-2017-1-0028 (MAR-S); the International Max Planck Research School 'Primary Metabolism and Plant Growth' at the Max Planck Institute of Molecular Plant Physiology (MA, ZN); the European Union's Horizon 2020 research and innovation program under the Marie Sklodowska-Curie grant agreement no. 751039 (ES-L); the program 'Plan Propio UCO' from University of Cordoba, Spain for postdoctoral Support (ES-L); the Carnegie Institution for Science (ARG); the Marie Curie Initial Training Network Accliphot FP7-PEOPPLE-2012-ITN; 316427 (SF, GF, DP); the Japan Society for the Promotion of Science, JSPS, for the grants-in-Aid for Scientific Research, KAKENHI, 21H04778 and 21H05040 (JM) and the German Research Foundation DFG HI 739/9.2 (MH).

Author contributions:

Conceptualization: MAR-S, ES-L, PR, GF, MH, ZN, JM, ARG, DP
Methodology: MAR-S, YY, GV, PR, ES-L, ZN, DP
Investigation: MAR-S, SF, YY, GV, RT, AK, AT, GK, GA, MA, FI
Supervision: GF, ZN, JM, ARG, DP
Writing—original draft: MAR-S, ARG, DP
Writing—review & editing: all authors

Competing interests: Authors declare that they have no competing interests.

Figures and Tables

Fig. 1. Acetate needs to be metabolized to inhibit LHCSR3 accumulation. WT, *icl*, *icl-C* and *dum11* strains were acclimated for 16 h in LL (15 µmol photons m^{-2} s^{-1}) in HSM; sparged with air (labelled as "air"); sparged with air and supplemented with 10 mM sodium acetate (labelled as "acet"); sparged with air enriched with 5% CO_2 (labelled as "CO_2"). After sampling for the LL conditions, light intensity was increased to 600 µmol photons m^{-2} s^{-1} (HL); samples were taken 1 h (RNA) or 4 h (protein) after exposure to HL. **a**, **c**. Accumulation of *LHCSR3* mRNA at the indicated conditions normalized to WT LL ctrl (n = 3 biological samples, mean ± s.d.). **b**, **d**. Immunoblot analyses of LHCSR3 and ATPB (loading control) under the indicated conditions**.** The p-values for the comparisons of acetate and CO_2 conditions to air are based on ANOVA Dunnett's multiple comparisons test of log10 transformed mRNA data as indicated in the graphs (*, $P < 0.005$, **, $P < 0.01$, ***, $P < 0.001$, ****, $P < 0.0001$, ns, not significant).

Fig. 2. LHCSR3 inhibition is driven by CO_2 derived from the metabolism of acetate. a, **b** mRNA accumulation of *LHCSR3* and *RHP1* and **c** concentration of sodium acetate in the growth medium in WT 137c and *icl* strains. Cells were acclimated overnight at LL (15 µmol photons m^{-2} s^{-1}) in HSM sparged with air. At t=0 cells either continued being sparged with air (labelled "air"); or sparged with air and supplemented with 10 mM sodium acetate (labelled "acet"); or sparged with air enriched with 5% CO_2 (labelled "CO_2"). The addition of acetate or CO_2 is indicated with a green mark on the x-axis. Samples were taken at t= 0, 1h, 4h and 8h. **d**, **e** mRNA accumulation of *LHCSR3* and *RHP1* and **f** concentration of sodium acetate in the growth medium in WT 137c and *icl* strains. Cells were acclimated overnight at LL (15 µmol photons m^{-2} s^{-1}) in HSM sparged with air; at t=0 light intensity was increased to 600 µmol photons m^{-2} s^{-1}. At t=1h cells either continued being sparged with air (labelled "air"); or sparged with air and supplemented with 10 mM sodium acetate (labelled "acet); or bubbled with air enriched with 5% CO_2 (labelled "CO_2"), always at 600 µmol photons m^{-2} s^{-1}. The time of addition of acetate or CO_2 is highlighted in green on the x-axis. Samples were taken at t= 0, 1h, 2h, 5h and 9h. (n = 3 biological samples, mean ± s.d.). The p-values for the comparisons of acetate and CO_2 conditions to air (LL; t = 1, 4, 8h, HL; t = 2, 5, 9h) are based on ANOVA Dunnett's multiple comparisons test of log10 transformed mRNA data as indicated in the graphs (*, $P < 0.005$, **, $P < 0.01$, ***, $P < 0.001$, ****, $P < 0.0001$, ns, not significant), following the color-code of the datasets.

Fig. 3. Kinetic resolution of photoprotective gene and protein expression at different light and CO_2 availabilities. Cells were acclimated overnight at LL (15 µmol photons m^{-2} s^{-1}) bubbled with air (labelled "air"). At t=0 the light intensity was raised to 600 µmol photons m^{-2} s^{-1} under air bubbling or bubbling with 5% CO_2 and mRNA and protein were followed for 25h. **a** *LHCSR1, LHCSR3* and *PSBS* mRNA accumulation. (n = 3 biological samples, mean ± s.d.). The p-values for the comparisons of CO_2 conditions to air for t=1, 4, 8, 24 and 25h are based on ANOVA Dunnett's multiple comparisons test of log10 transformed mRNA data as indicated in the graphs (*, $P < 0.005$, **, $P < 0.01$, ***, $P < 0.001$, ****, $P < 0.0001$, ns, not significant). **b** Immunoblot analyses of LHCSR1, LHCSR3 and ATPB (loading control).

Fig. 4. Cross-talk of responses to HL and low-CO_2. a WT, *icl* and *icl-C* strains were acclimated for 16 h in LL in HSM; bubbled with air (labelled as "air"); bubbled with

air and HSM supplemented with 10 mM sodium acetate (labelled as "acet); bubbled with air enriched with 5% CO_2 (labelled as "CO_2"). After sampling for the LL conditions, light intensity was increased (HL); samples were taken after 1 h. Accumulation of mRNA of selected CCM genes at the indicated conditions normalized to WT LL air. Please note that these data derive from analyses of the RNA samples of the experiment described in Fig. 1. (n = 3 biological samples, mean ± s.d.). The p-values for the comparisons of CO_2 and acetate conditions to air are based on ANOVA Dunnett's multiple comparisons test of log10 transformed mRNA data as indicated in the graphs (*, P < 0.005, **, P < 0.01, ***, P < 0.001, ****, P < 0.0001, ns, not significant). **b** CC-125 WT, *cia5* and *cia5*-c strains were acclimated for 16 h in LL (15 µmol photons m^{-2} s^{-1}) in HSM bubbled with air (labelled as "LL"); after sampling for the LL conditions, light intensity was increased to 600 µmol photons m^{-2} s^{-1} (HL); samples were taken after 1h (RNA) and 4h (protein and photosynthesis measurements). Accumulation of mRNA of genes at the indicated conditions were normalized to WT LL ctrl. (n = 3 biological samples, mean ± s.d.). The p-values for the comparisons of WT with *cia5* and *cia5* with *cia5-C* are based on ANOVA Dunnett's multiple comparisons test of log10 transformed mRNA data as indicated in the graphs. **c** Immunoblot analyses of LHCSR3, LHCSR1 and ATPB (loading control) under the indicated conditions; PSBS was non-detectable at these experimental conditions. **d** qE of WT, *cia5* and *cia5-C* under LL and HL conditions (n = 3 biological samples, mean ± s.d.). The statistical analyses (ordinary one-way ANOVA test) are shown in the graph. Raw fluorescence and NPQ curves can be seen in **Supplementary Fig. 4.**

Fig. 5. Low CO_2 levels can trigger qE and CCM genes in the absence of light. WT, *cia5* and *cia5-C* cells were bubbled with air overnight in darkness; next day air bubbling was either maintained or replaced by CO_2-limited-air bubbling in the darkness or in the presence of 600 µmol photons m^{-2} s^{-1} light. Sampling was performed after 1 h (RNA) or 4 h (protein). **a** mRNA accumulation of *LHCSR3.1* (qE gene) and *CAH4, LCIA, LCI1* (CCM genes) in WT, *cia5* and *cia5-C*. Data were normalized to WT air dark; (n = 3 biological samples, mean ± s.d.). The p-values for the comparisons of WT with *cia5* and *cia5* with *cia5-C* are based on ANOVA Dunnett's multiple comparisons test of log10 transformed mRNA data as indicated in the graphs (*, P < 0.005, **, P < 0.01, ***, P < 0.001, ****, P < 0.0001, ns, not significant). **b** Immunoblot analyses of LHCSR3 and ATPB (loading control) under the indicated conditions. **c** Immunoblot analyses of LHCSR3 and ATPB (loading control) of WT samples presented in **b**. Above the immunoblot shown are the amount of protein loaded per lane and the quantification of LHCSR3 protein accumulation (calculated as LHCSR3 /ATPB ratio) normalized to the air dark conditions. **d** CO_2 concentration measured in the air stream coming out of the headspace of a column filled with 50 mL of HSM, sparged with air under HL. The two arrows in the graph indicate the addition of cells or DCMU. **e** WT cells were acclimated to LL HSM overnight shaken in flasks; the next day they were exposed to 300 µmol photons m^{-2} s^{-1} light in the presence or absence of 40 µM DCMU, shaken in flasks without or with sparging with $VLCO_2$. Samples were taken after 1 h. Presented are mRNA accumulation of *LHCSR3*, *CAH4*, *LCIA*. Data were normalized to LL (shown as dotted line in graph); n = 3 biological samples, mean ± s.d.

Fig. 6. CO_2 -and light-dependent signals converge to regulate photoprotection and CCM in *Chlamydomonas*. The intracellular levels of CO_2, defined by the equilibrium between CO_2 fixation in chloroplasts and the generation of CO_2 by mitochondrial metabolism (e.g. acetate assimilation) is the key determinant of the

regulation of gene expression controlling two major processes of photosynthetic organisms: CCM and photoprotection. Changes in light availability have a direct impact on intracellular CO_2 levels; exposure to HL increases CO_2 fixation rates leading to depletion of CO_2 and to activation of not only photoprotection- but also CCM-related genes. Conversely, depletion of CO_2 is sufficient to drive high expression levels of CCM genes and *LHCSR3* even in complete darkness (indicated by the black arrows). High CO_2 levels, either exogenously supplied by sparging or metabolically produced via acetate metabolism or by inhibiting photosynthetic electron flow using DCMU, repress *LHCSR3* and CCM genes while at the same time they stabilize LHCSR1 protein levels. The close interconnection of photoprotection and CCM is further corroborated by the fact that CIA5, the regulator of expression of genes associated with the CCM, also exerts control over *LHCSR3* and to a lesser extent over *PSBS* mRNA levels and acts as repressor of LHCSR1 protein accumulation. Independent of CIA5, light strongly impacts expression of all of these photoprotective genes (yellow arrows). This impact can be the consequence of both photoperception (e.g. phototropin) and the production of reactive oxygen levels.

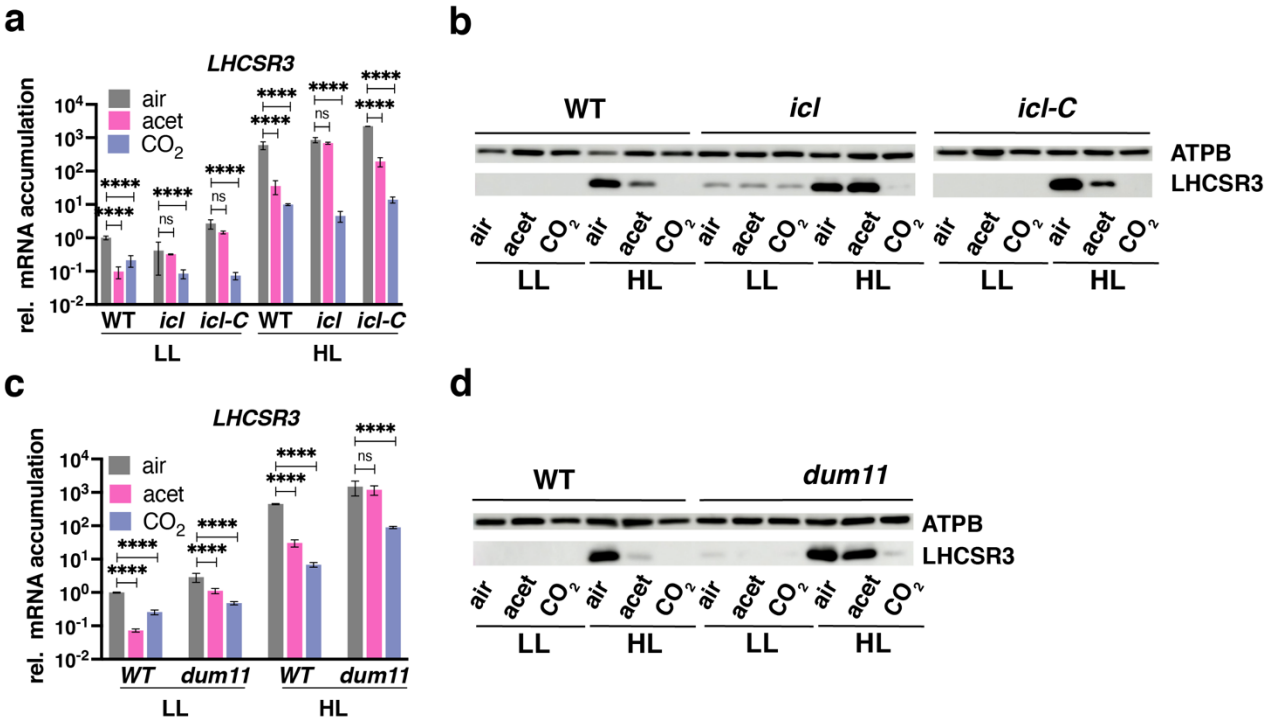

Figure 1: Acetate needs to be metabolized to inhibit LHCSR3 accumulation. 137c WT, *icl*, *icl-C* and *dum11* strains were acclimated for 16 h in LL (15 µmol photons m^{-2} s^{-1}) in HSM; sparged with air (labelled as "air"); sparged with air and supplemented with 10 mM sodium acetate (labelled as "acet"); sparged with air enriched with 5% CO_2 (labelled as "CO_2"). After sampling for the LL conditions, light intensity was increased to 600 µmol photons m^{-2} s^{-1} (HL); samples were taken 1 h (RNA) or 4 h (protein) after exposure to HL. **a**, **c**. Accumulation of *LHCSR3* mRNA at the indicated conditions normalized to WT LL ctrl (n = 3 biological samples, mean ± s.d.). **b**, **d**. Immunoblot analyses of LHCSR3 and ATPB (loading control) under the indicated conditions**.** The p-values for the comparisons of acetate and CO_2 conditions to air are based on ANOVA Dunnett's multiple comparisons test of log10 transformed mRNA data as indicated in the graphs (*, P < 0.005, **, P < 0.01, ***, P < 0.001, ****, P < 0.0001, ns, not significant).

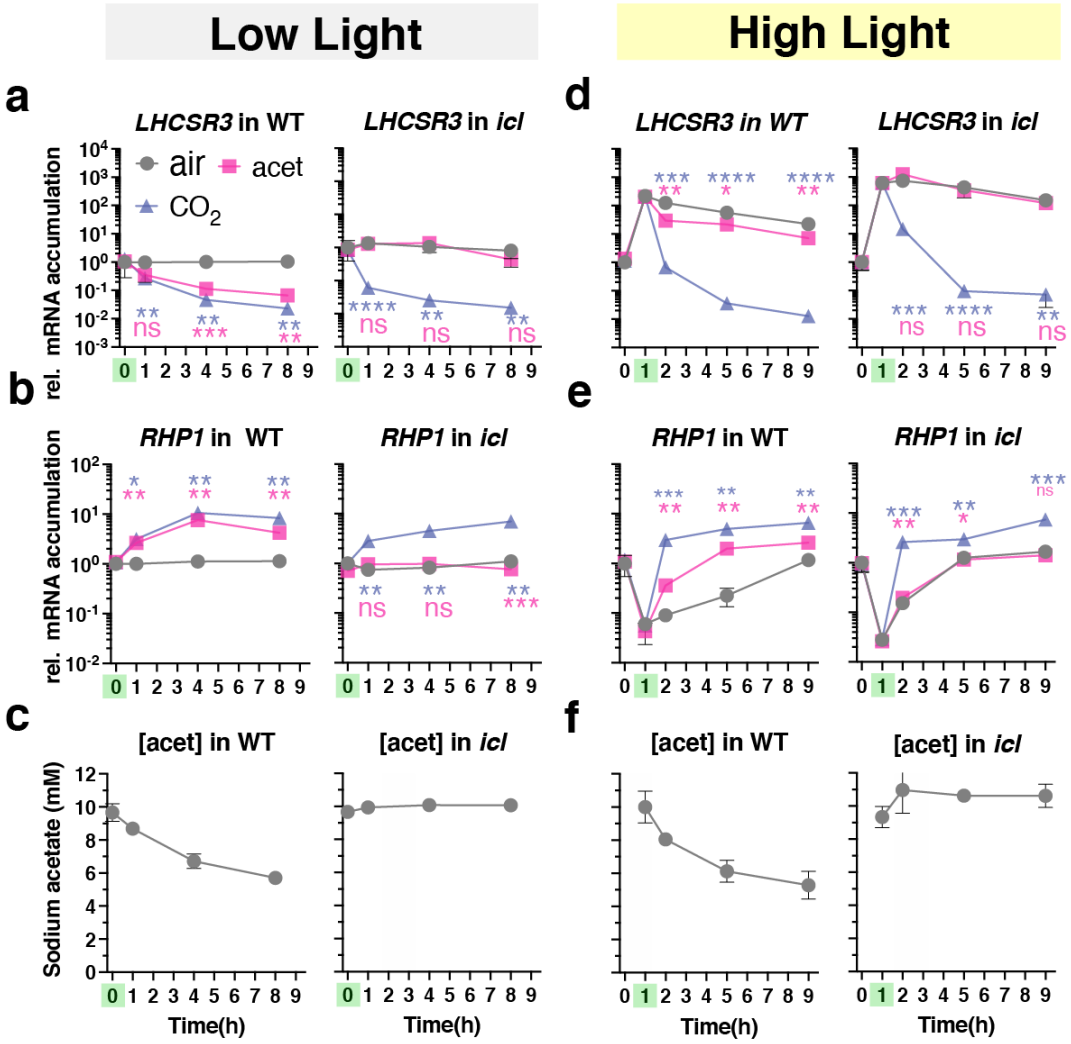

Figure 2: LHCSR3 inhibition is driven by CO_2 derived from the metabolism of acetate.
a, **b** mRNA accumulation of *LHCSR3* and *RHP1* and **c** concentration of sodium acetate in the growth medium in WT 137c and *icl* strains. Cells were acclimated overnight at LL (15 µmol photons m^{-2} s^{-1}) in HSM sparged with air. At t=0 cells either continued being sparged with air (labelled "air"); or sparged with air and supplemented with 10 mM sodium acetate (labelled "acet"); or sparged with air enriched with 5% CO_2 (labelled "CO_2"). The addition of acetate or CO_2 is indicated with a green mark on the x-axis. Samples were taken at t= 0, 1h, 4h and 8h. **d**, **e** mRNA accumulation of *LHCSR3* and *RHP1* and **f** concentration of sodium acetate in the growth medium in WT 137c and *icl* strains. Cells were acclimated overnight at LL (15 µmol photons m^{-2} s^{-1}) in HSM sparged with air; at t=0 light intensity was increased to 600 µmol photons m^{-2} s^{-1}. At t=1h cells either continued being sparged with air (labelled "air"); or sparged with air and supplemented with 10 mM sodium acetate (labelled "acet); or bubbled with air enriched with 5% CO_2 (labelled "CO_2"), always at 600 µmol photons m^{-2} s^{-1}. The time of addition of acetate or CO_2 is highlighted in green on the x-axis. Samples were taken at t= 0, 1h, 2h, 5h and 9h. (n = 3 biological samples, mean ± s.d.). The p-values for the comparisons of acetate and CO_2 conditions to air (LL; t = 1, 4, 8h, HL; t = 2, 5, 9h) are based on ANOVA Dunnett's multiple comparisons test of log10 transformed mRNA data as indicated in the graphs (*, $P < 0.005$, **, $P < 0.01$, ***, $P < 0.001$, ****, $P < 0.0001$, ns, not significant), following the color-code of the datasets.

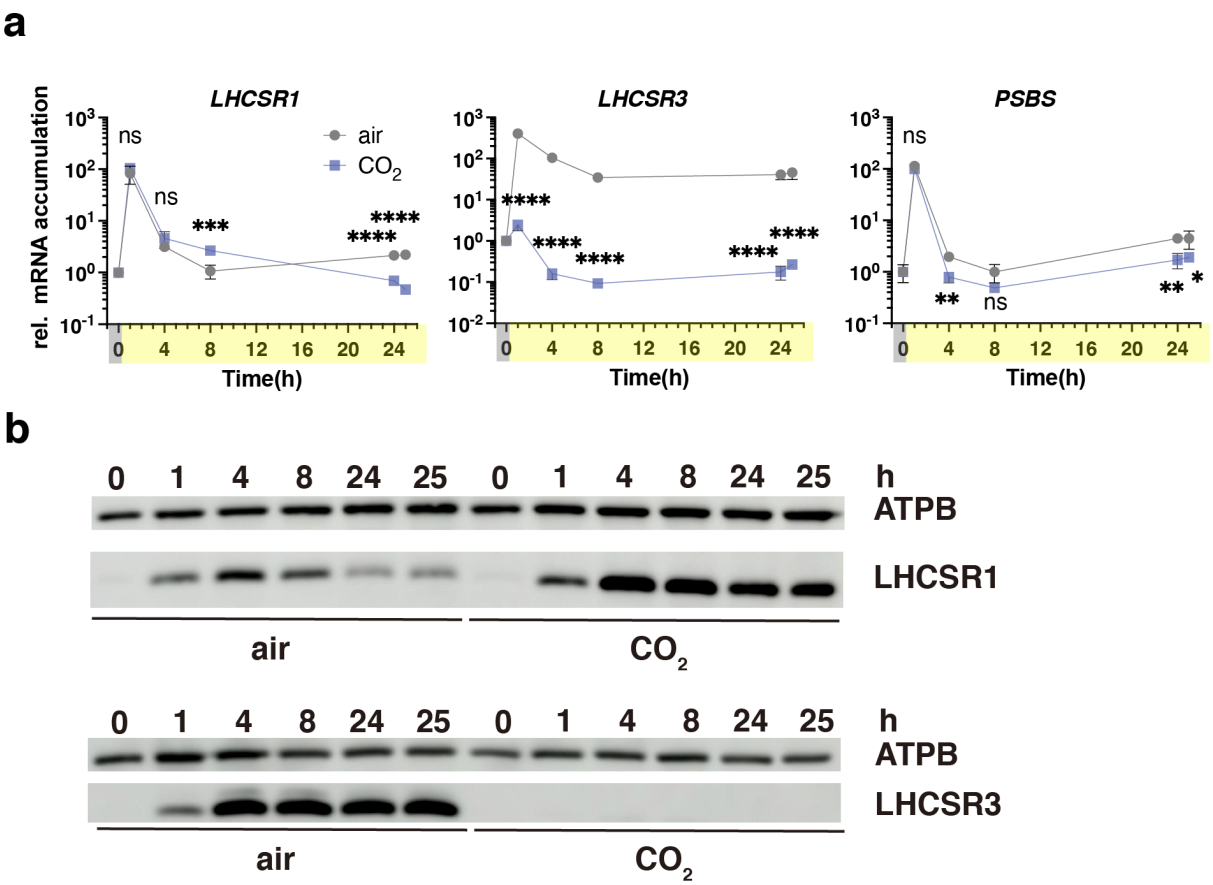

Figure 3: Kinetic resolution of photoprotective gene and protein expression at different light and CO_2 availabilities. Cells were acclimated overnight at LL (15 µmol photons m^{-2} s^{-1}) bubbled with air (labelled "air"). At t=0 the light intensity was raised to 600 µmol photons m^{-2} s^{-1} under air bubbling or bubbling with 5% CO_2 and mRNA and protein were followed for 25h. **a** *LHCSR1, LHCSR3* and *PSBS* mRNA accumulation. (n = 3 biological samples, mean ± s.d.). The p-values for the comparisons of CO_2 conditions to air for t=1, 4, 8, 24 and 25h are based on ANOVA Dunnett's multiple comparisons test of log10 transformed mRNA data as indicated in the graphs (*, $P < 0.005$, **, $P < 0.01$, ***, $P < 0.001$, ****, $P < 0.0001$, ns, not significant). **b** Immunoblot analyses of LHCSR1, LHCSR3 and ATPB (loading control).

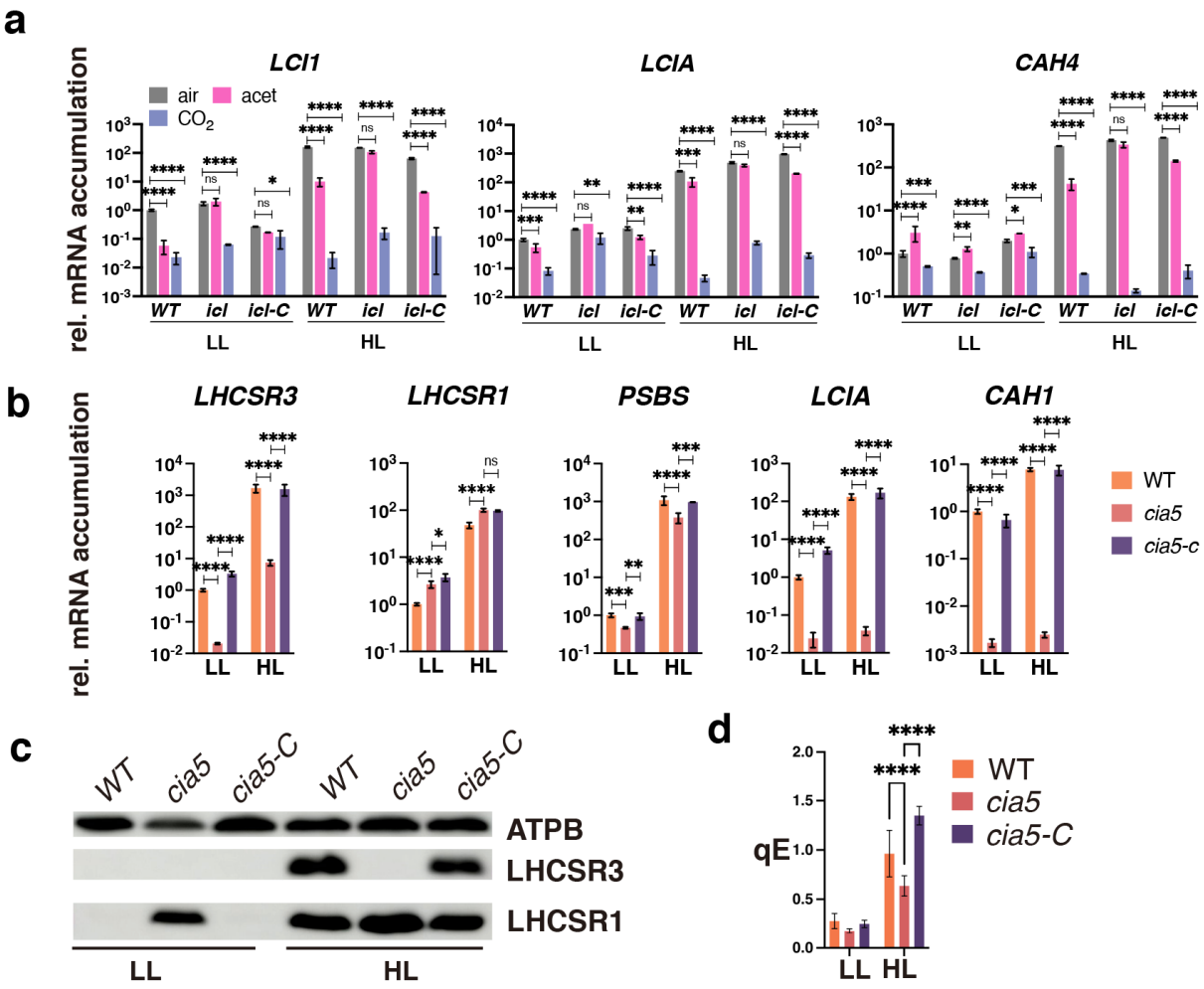

Figure 4: Cross-talk of responses to HL and low-CO_2.
a 137c WT, *icl* and *icl-C* strains were acclimated for 16 h in LL in HSM; bubbled with air (labelled as "air"); bubbled with air and HSM supplemented with 10 mM sodium acetate (labelled as "acet"); bubbled with air enriched with 5% CO_2 (labelled as "CO_2"). After sampling for the LL conditions, light intensity was increased (HL); samples were taken after 1 h. Accumulation of mRNA of selected CCM genes at the indicated conditions normalized to WT LL air. Please note that these data derive from analyses of the RNA samples of the experiment described in Fig. 1. (n = 3 biological samples, mean ± s.d.). The p-values for the comparisons of CO_2 and acetate conditions to air are based on ANOVA Dunnett's multiple comparisons test of log10 transformed mRNA data as indicated in the graphs (*, P < 0.005, **, P < 0.01, ***, P < 0.001, ****, P < 0.0001, ns, not significant). **b** CC-125 WT, *cia5* and *cia5*-c strains were acclimated for 16 h in LL (15 µmol photons m^{-2} s^{-1}) in HSM bubbled with air (labelled as "LL"); after sampling for the LL conditions, light intensity was increased to 600 µmol photons m^{-2} s^{-1} (HL); samples were taken after 1h (RNA) and 4h (protein and photosynthesis measurements). Accumulation of mRNA of genes at the indicated conditions were normalized to WT LL ctrl. (n = 3 biological samples, mean ± s.d.). The p-values for the comparisons of WT with *cia5* and *cia5* with *cia5-C* are based on ANOVA Dunnett's multiple comparisons test of log10 transformed mRNA data as indicated in the graphs. **c** Immunoblot analyses of LHCSR3, LHCSR1 and ATPB (loading control) under the indicated conditions; PSBS was non-detectable at these experimental conditions. **d** qE of WT, *cia5* and *cia5-C* under LL and HL conditions (n = 3 biological samples, mean ± s.d.). The statistical analyses (ordinary one-way ANOVA test) are shown in the graph. Raw fluorescence and NPQ curves can be seen in **Fig. S4.**

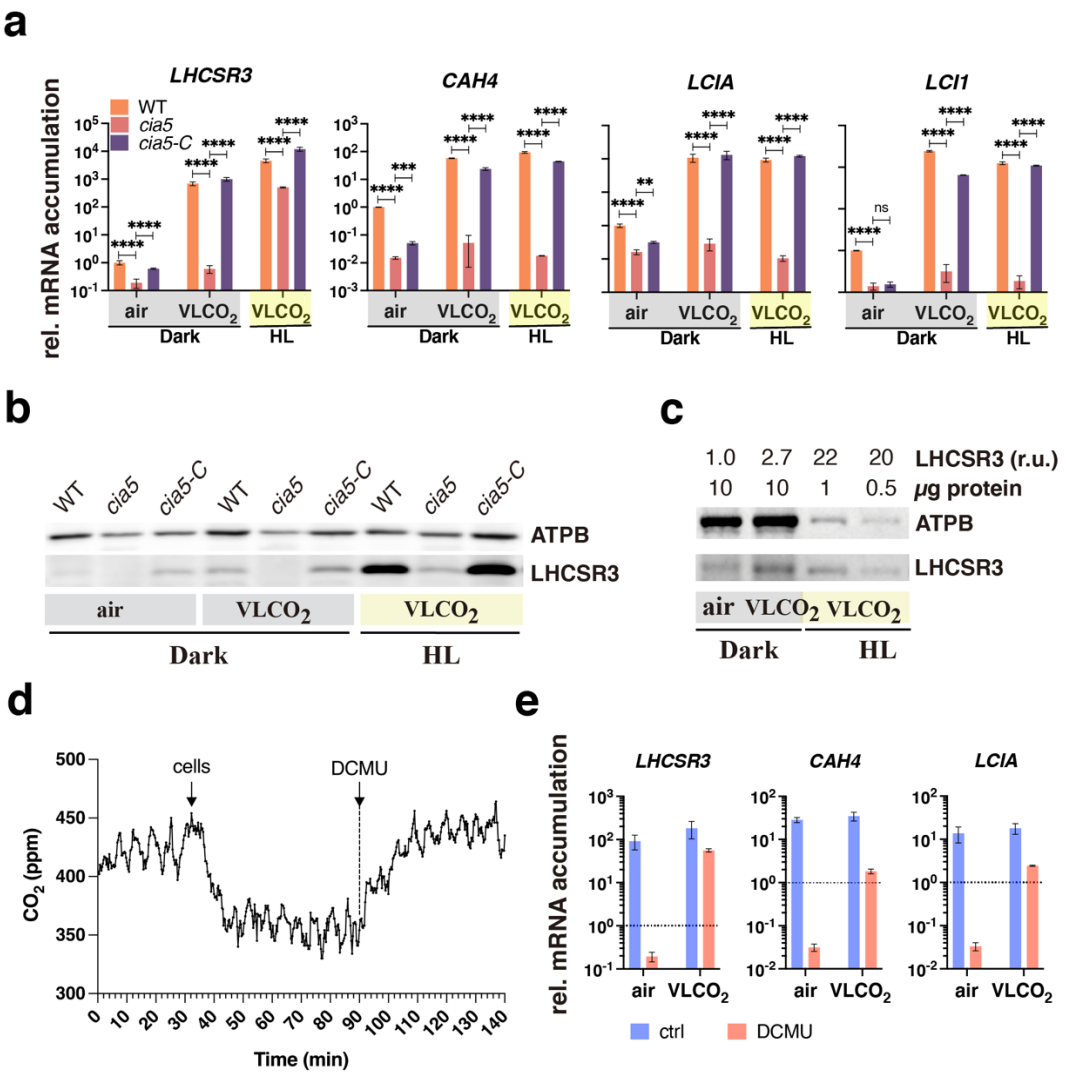

Figure 5: Low CO_2 levels can trigger qE and CCM genes in the absence of light. WT, *cia5* and *cia5-C* cells were bubbled with air overnight in darkness; next day air bubbling was either maintained or replaced by CO_2-limited-air bubbling in the darkness or in the presence of 600 µmol photons m^{-2} s^{-1} light. Sampling was performed after 1 h (RNA) or 4 h (protein).
a mRNA accumulation of *LHCSR3.1* (qE gene) and *CAH4, LCIA, LCI1* (CCM genes) in WT, *cia5* and *cia5-C*. Data were normalized to WT air dark; (n = 3 biological samples, mean ± s.d.). The p-values for the comparisons of WT with *cia5* and *cia5* with *cia5-C* are based on ANOVA Dunnett's multiple comparisons test of log10 transformed mRNA data as indicated in the graphs (*, P < 0.005, **, P < 0.01, ***, P < 0.001, ****, P < 0.0001, ns, not significant). **b** Immunoblot analyses of LHCSR3 and ATPB (loading control) under the indicated conditions. **c** Immunoblot analyses of LHCSR3 and ATPB (loading control) of WT samples presented in **b**. Above the immunoblot shown are the amount of protein loaded per lane and the quantification of LHCSR3 protein accumulation (calculated as LHCSR3 /ATPB ratio) normalized to the air dark conditions. **d** CO_2 concentration measured in the air stream coming out of the headspace of a column filled with 50 mL of HSM, sparged with air under HL. The two arrows in the graph indicate the addition of cells or DCMU. **e** WT cells were acclimated to LL HSM overnight shaken in flasks; the next day they were exposed to 300 µmol photons m^{-2} s^{-1} light in the presence or absence of 40 µM DCMU, shaken in flasks without or with sparging with $VLCO_2$. Samples were taken after 1 h. Presented are mRNA accumulation of *LHCSR3*, *CAH4*, *LCIA*. Data were normalized to LL (shown as dotted line in graph); n = 3 biological samples, mean ± s.d.

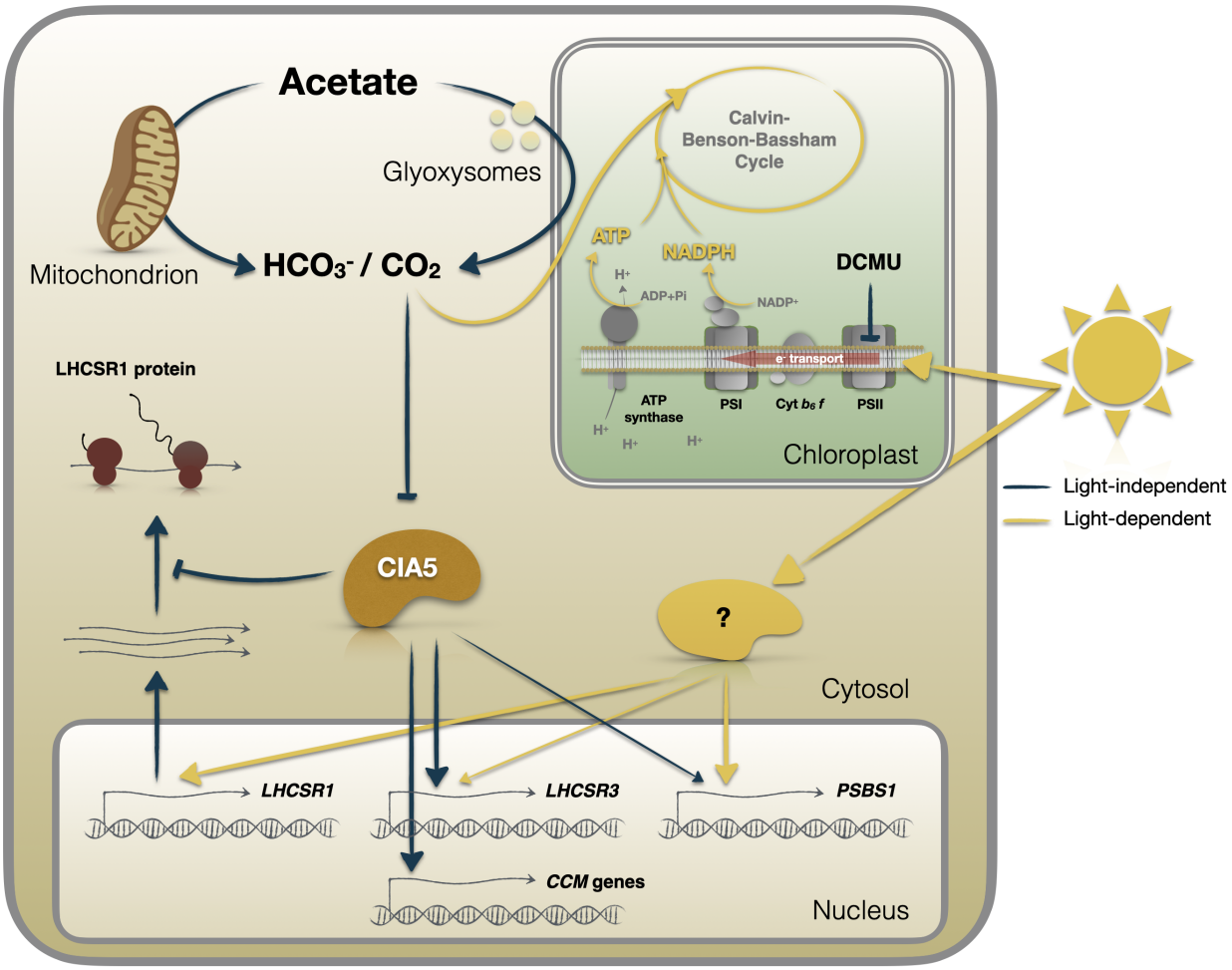

Figure 6. CO_2 -and light-dependent signals converge to regulate photoprotection and CCM in Chlamydomonas. The intracellular levels of CO_2, defined by the equilibrium between CO_2 fixation in chloroplasts and the generation of CO_2 by mitochondrial metabolism (e.g. acetate assimilation) is the key determinant of the regulation of gene expression controlling two major processes of photosynthetic organisms: CCM and photoprotection. Changes in light availability have a direct impact on intracellular CO_2 levels; exposure to HL increases CO_2 fixation rates leading to depletion of CO_2 and to activation of not only photoprotection- but also CCM-related genes. Conversely, depletion of CO_2 is sufficient to drive high expression levels of CCM genes and *LHCSR3* even in complete darkness (indicated by the black arrows). High CO_2 levels, either exogenously supplied by sparging or metabolically produced via acetate metabolism or by inhibiting photosynthetic electron flow using DCMU, repress *LHCSR3* and CCM genes while at the same time they stabilize LHCSR1 protein levels. The close interconnection of photoprotection and CCM is further corroborated by the fact that CIA5, the regulator of expression of genes associated with the CCM, also exerts control over *LHCSR3* and to a lesser extent over *PSBS* mRNA levels and acts as repressor of LHCSR1 protein accumulation. Independent of CIA5, light strongly impacts expression of all of these photoprotective genes (yellow arrows). This impact can be the consequence of both photoperception (e.g. phototropin) and the production of reactive oxygen levels.

Supplementary Materials for

Photoprotection is regulated by light-independent CO_2 availability

M. Águila Ruiz-Sola[1,†,‡], Serena Flori[1,†], Yizhong Yuan[1,†], Gaelle Villain[1], Emanuel Sanz-Luque[2,3], Petra Redekop[2], Ryutaro Tokutsu[4], Anika Kueken[5,6], Angeliki Tsichla[1], Georgios Kepesidis[1], Guillaume Allorent[1], Marius Arend[5,6], Fabrizio Iacono[1], Giovanni Finazzi[1], Michael Hippler[7], Zoran Nikoloski[5,6], Jun Minagawa[4], Arthur R. Grossman[2], Dimitris Petroutsos[1,*]

[*]Corresponding Author. Email: dimitris.petroutsos@cea.fr

This PDF file includes:

Supplementary Note
Supplementary References related to Supplementary Note
Supplementary Figs 1 to 9
Supplementary Tables 1 to 3

Other Supplementary Materials for this manuscript include the following:

Supplementary Data 1 (to be downloaded as excel file)

Supplementary Note

We used flux balance analysis (FBA)[1] to test whether the genome-scale model of *Chlamydomonas i*Cre1355[2] could accurately predict the specific growth rates (generation time) of the *icl* and *dum11* strains under autotrophic LL, autotrophic HL and mixotrophic (acetate) HL conditions. We first constrained the specific growth rates of WT to the measured values under LL and HL[3] and determined the respective minimum photon uptake supporting the specific growth rates (Methods). Assuming that the photon uptake is not altered in the mutants, the determined minimum photon uptake was then used as a bound in the FBA-based prediction of generation times for the *icl* and *dum11* strains. In line with the experimentally observed values, we found that the predicted generation times for the *icl* and *dum11* strains grown autotrophically under LL did not differ from those of LL grown WT cells (**Supplementary Table 1**). In comparison to LL conditions, the predicted generation time of the *icl* and *dum11* strains grown autotrophically under HL decreased by 1.8- and 1.6-fold, respectively, which was also similar to that of WT cells (**Supplementary Table 1**). However, the predicted generation time for the WT grown under mixotrophic HL conditions further declined by 2-fold, to 11 h while the mutants under mixotrophic HL conditions had a generation time similar to that observed under autotrophic HL conditions (19 h, **Supplementary Table 1**). These findings showed that the FBA-based modeling with the condition-specific constraints can reproduce experimental findings regarding strain- and condition-specific generation times.

We next examined whether the CO_2-producing reactions show flux differences between the WT and the mutant strains under the specific growth conditions used. To this end, we followed two strategies, one based on the differences in the flux ranges and another based on the differences in the sampled steady-state flux distributions. By using the first strategy, we found a number of reactions whose steady-state flux ranges did not overlap between the WT and modelled mutants under the investigated conditions (**Supplementary Data 1a**), suggesting clear redistribution of fluxes between WT and mutant. The second strategy allowed us to identify reactions that showed both significant differences in the distributions of the sampled flux values, using the Kolmogorov-Smirnov test, and significant difference in means between WT and the mutants, based on t-tests (**Supplementary Data 1b**). The Fisher's exact test was in turn used to assess if the set of reactions showing differences are enriched with CO_2-producing reactions. Our findings showed that there is a significant difference (p-value = 0.003) in the flux of CO_2-producing reactions between WT and mutants for mixotrophic growth under HL conditions; analogous conclusions were made when only focusing on the CO_2-producing reactions in the chloroplast (p-value= 6.4e-04; **Supplementary Table 2**). However, this could not be observed under LL and HL photoautotrophic conditions.

Prompted by these findings, we interrogated whether or not changes in flux are associated with changes in the internal CO_2 concentration. Since FBA cannot be used to predict concentrations of metabolites, we used a technique employed in the design of metabolic engineering strategies to modulate the production (and hence concentration) of a metabolite of interest. This technique entails insertion of a synthetic 'demand' reaction for the metabolite of interest, which exports the metabolite out of the network. In our case, we inserted a demand reaction for CO_2 from the chloroplast to the environment, and used its maximum flux, at the specific condition associated with strain-specific-growth constraints, as a proxy for intracellular CO_2. We then inspected the condition-specific flux through the added demand reaction for different combinations of CO_2 and acetate uptake rates (**Supplementary Fig. 1**). We observed the same flux pattern for the CO_2 demand reaction with varying rates of CO_2 uptake from the environment across all strains under autotrophic LL and HL. We hypothesized that under LL more CO_2 can accumulate because of slow carbon fixation in comparison to HL conditions, where CO_2 fixation is faster. In support of this hypothesis, we found that all strains showed larger flux through the CO_2 demand reaction, as a proxy for the internal CO_2 levels, under LL than HL conditions when the CO_2 uptake rates were

larger than 0.2 mmol/gDW/h (**Supplementary Fig. 1a-c**). Under mixotrophic HL conditions, with the assumption of no change in CO_2 uptake from the environment and a decrease of at least 10% in acetate uptake for both mutants in comparison to WT, we found that both the *icl* and *dum11* mutants showed smaller flux through the CO_2 demand reaction, i.e. lower internal CO_2 concentration than what was observed for WT (**Supplementary Fig. 1d-f**). Furthermore, the same pattern holds with the assumption that CO_2 uptake under HL is at least as high as under LL and acetate uptake rates are below 0.3 mmol/gDW/h. In contrast, only few combinations of CO_2 and acetate uptake rates for which the mutant strains showed CO_2 demand that is similar under autotrophic LL and mixotrophic HL conditions, but larger than the CO_2 demand in the WT under auxotrophic LL conditions. Therefore, we concluded that larger CO_2 demand flux under autotrophic LL than HL conditions for each strain can be observed with the assumptions that: (i) the CO_2 uptake was not affected by the mutation, (ii) CO_2 uptake is the same for phototrophic HL and mixotrophic HL, (iii) CO_2 uptake under HL is at least as high as under LL and (iv) the acetate uptake rate is low (i.e., below 0.3 mmol/gDW/h) for the mutants (as indicated in **Fig. 2c** and **f**). Moreover, under mixotrophic HL conditions, both mutants exhibited CO_2 demand rates that were smaller than those under autotrophic LL conditions. In contrast, the WT showed a marked increase in the CO_2 demand flux under mixotrophic HL conditions in comparison to autotrophic LL and HL, indicating higher internal CO_2 concentrations in the presence of acetate. In conclusion, genome-scale metabolic modelling supports the hypothesis that there are changes in the internal CO_2 concentration under autotrophic and mixotrophic growth conditions at different light intensities. These changes are congruent with the changes in the accumulation of *LHCSR3* transcripts under the different media conditions and in the WT and mutant cells.

Condition and strain-specific metabolic models

Simulations of different strain, $s = \{WT, icl, dum11\}$, and conditions, $c = \{LL, HL, HL + acetate\}$, are based on the genome-scale metabolic network reconstruction *i*Cre1355 of *Chlamydomonas reinhardtii* metabolism [2]. The reconstruction provides the underlying structure of the metabolic reactions captured in the stoichiometric matrix, N, where rows correspond to metabolites and columns denote reactions. Each entry in the stoichiometric matrix indicates the molarity with which a metabolite is consumed (negative value) or produced (positive value) by the respective reaction. In addition, condition-specific lower and upper bounds on reaction flux, $v_{min}^{WT,c} \leq v \leq v_{max}^{WT,c}$, for autotrophic (LL, HL) and mixotrophic (HL + acetate) growth are provided with the model. To obtain models for the mutants *icl* and *dum11* we used the gene-protein-reaction rules, provided along the network reconstruction, to identify reactions related to knocked-out genes Cre06.g282800 and CreMt.g000300, respectively. Gene Cre06.g282800 relates to reaction isocitrate lyase and therefore, flux through this reaction is blocked in the simulations of *icl*. For the mutant *dum11* the knocked-out gene CreMt.g000300 was not part of the model. However, it is known that this mutant shows no activity of respiratory complex III, therefore the corresponding model reaction was blocked in the simulation of *dum11*.

The strain and condition-specific simulations, together with constraint-based modeling approaches were used to investigate steady state flux distributions, v. First, we used the WT model under autotrophic conditions to obtain estimates for photon uptake rates under LL and HL conditions, later used as constraints in the mutant models and for the WT model under HL + acetate condition. Therefore, we take generation time (g) of *Chlamydomonas* WT under LL and HL measured by Bonente et al. [3] and converted them into growth rates (μ) assuming that $g = \frac{log(2)}{\mu}$. The respective growth rate was used to constrain the WT model under LL and HL conditions. To estimate photon uptake in units mmol gDW^{-1} h^{-1} under low and high light conditions, we found the minimum photon uptake rate that supports the condition-specific WT growth rate (bio_c^{WT}) under LL and HL,

respectively (Eq. 1). The resulting photon uptake rates were used as constraints for the simulation of mutants as well as under HL mixotrophic growth for the WT (were no measured growth rates were available). The following is the linear program that we solve:

$$
\begin{aligned}
& z^{c}_{photon_{uptake}} = \min v_{photon_{uptake}} \\
& s.t. \\
& Nv = 0 \\
& v_{bio} = bio^{WT}_{c} \\
& v^{WT,c}_{min} \leq v \leq v^{WT,c}_{max}.
\end{aligned}
\qquad (1)
$$

Next, we used the observation that mutants cannot grow on acetate in darkness to find acetate uptake rates that allow simulation of no growth in darkness for both mutants. Acetate uptake for both mutants were reduced by 90% in comparison to the WT rate (0.2 mmol gDW^{-1} h^{-1} in mutants and 2 mmol gDW^{-1} h^{-1} in WT), since this rate is the minimum uptake rate for which no growth was simulated in darkness.

Flux balance analysis

To simulate maximal growth rates for WT under HL + acetate as well as *icl* and *dum11* under LL, HL and HL + acetate respectively, we applied flux balance analysis (FBA; [4,5]) We found maximal growth rates (Eq. 2) by using the model biomass reaction for mixotrophic and photoautotrophic growth and the respective light constraints. Moreover, acetate uptake for mutant models under HL + acetate was set to 0.2 mmol gDW^{-1} h^{-1}, the minimum acetate uptake rate for which no growth was simulated in darkness. To this end, we used the following program:

$$
\begin{aligned}
& z^{s,c}_{bio} = \max v_{bio} \\
& s.t. \\
& Nv = 0 \\
& v_{photon_{uptake}} = z^{c}_{photon_{uptake}} \\
& v^{s,c}_{min} \leq v \leq v^{s,c}_{max}.
\end{aligned}
\qquad (2)
$$

Flux ranges

The solution of the linear programming problem in Eq. (2), above, is the maximum growth, i.e. flux value of the strain and condition-specific biomass reaction, $z^{s,c}_{bio}$. Flux variability analysis (FVA) allows determining the minimum and the maximum value of flux that a given reaction can carry while ensuring maximum flux through the biomass reaction [6]. These values can be obtained by solving the following linear program for a given reaction i. The flux through the condition-specific biomass reaction was set to 99% of the optimum to avoid numerical instabilities. To conduct FVA, we solved the following linear programs:

$$
\begin{aligned}
& z^{s,c}_{i,\max(\min)} = \max(\min)\, v_i \\
& \text{s.t.} \\
& Nv = 0 \\
& v_{photon_{uptake}} = z^{c}_{photon_{uptake}} \\
& v^{s,c}_{min} \leq v \leq v^{s,c}_{max} \\
& v_{bio} = z^{s,c}_{bio} * 0.99
\end{aligned}
\qquad (3)
$$

Moreover, we sample 5000 feasible steady-state flux distributions from the flux cone of the strain and condition-specific models by applying the function *gpSampler* from the COBRA toolbox [7]. Here, too, biomass was set to 99% of its optimum.

Maximize CO_2 demand

We introduce a demand reaction for CO_2 in the chloroplast and maximize its flux given constraints described in the linear program in Eq. (4), which include the fixation of condition-specific growth as well as uptake rates of CO_2 and acetate. The obtained flux through CO_2 demand will serve as a proxy for internal CO_2 concentration in the chloroplast:

$$
\begin{aligned}
& z^c = \max\ v_{CO_2\ demand} \\
& \text{s.t.} \\
& Nv = 0 \\
& v_{photon_{uptake}} = z^c_{photon_{uptake}} \\
& v_{CO_2\ uptake} = CO_2\ uptake^c \\
& v_{acetate\ uptake} = acetate\ uptake^c \\
& v^{s,c}_{min} \le v \le v^{s,c}_{max} \\
& v_{bio} = z^{s,c}_{bio} * 0.99
\end{aligned}
\qquad (4)
$$

Supplementary References

1. Varma, A. & Palsson, B. O. Metabolic capabilities of Escherichia coli: I. synthesis of biosynthetic precursors and cofactors. *J. Theor. Biol.* **165,** 477–502 (1993).
2. Imam, S. *et al.* A refined genome-scale reconstruction of Chlamydomonasmetabolism provides a platform for systems-level analyses. *Plant J.* **84,** 1239–1256 (2015).
3. Bonente, G., Pippa, S., Castellano, S., Bassi, R. & Ballottari, M. Acclimation of Chlamydomonas reinhardtii to different growth irradiances. *J. Biol. Chem.* (2011). doi:10.1074/jbc.M111.304279
4. Orth, J. D., Thiele, I. & Palsson, B. Ø. What is flux balance analysis? *Nat. Biotechnol.* **28,** 245–248 (2010).
5. Bordbar, A., Monk, J. M., King, Z. A. & Palsson, B. Ø. Constraint-based models predict metabolic and associated cellular functions. *Nat. Rev. Genet.* **15,** 107–120 (2014).
6. Gudmundsson, S. & Thiele, I. Computationally efficient flux variability analysis. *BMC Bioinformatics* **11,** 489–3 (2010).
7. Heirendt, L. *et al.* Creation and analysis of biochemical constraint-based models using the COBRA Toolbox v.3.0. *Nature Protocols* **14,** 639–702 (2019).

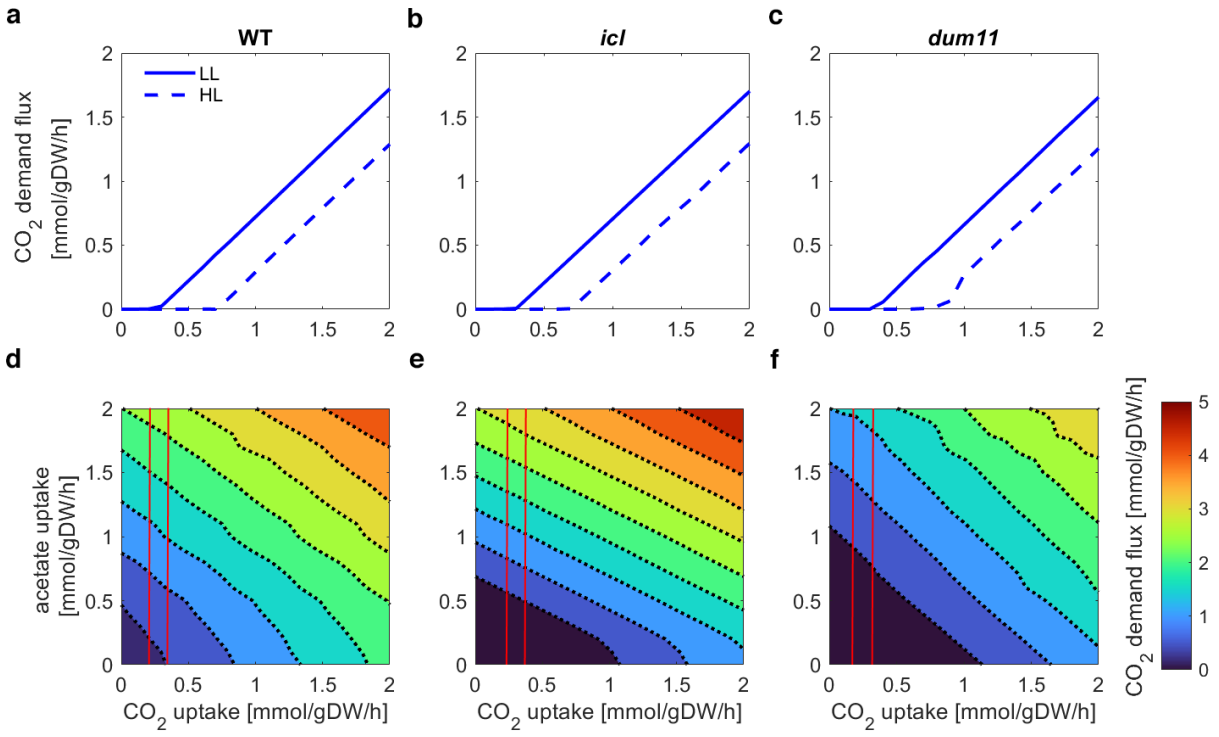

Supplementary Fig. 1: Large-scale metabolic modeling supports the change in internal CO_2 concentration under mixotrophic conditions. The maximum flux through the CO_2 demand reaction is used as a proxy for concentration of free CO_2 in the chloroplast. **a-c** Flux through CO_2 demand reaction under low light (LL) and high light (HL) for varying CO_2 uptake rates for wild type (wt), *icl*, and *dum11*. **d-f** Contour plots of flux through CO_2 demand reaction under HL and acetate for varying CO_2 and acetate uptake rates for the three respective strains.
The area between the two red lines indicates combinations of CO_2 and acetate uptake rates that show (i) in the case of mutants: CO_2 demand level under HL acetate conditions similar to those under LL conditions and (ii) in the case of the WT: CO_2 demand level under HL acetate conditions above what is observed under LL conditions.

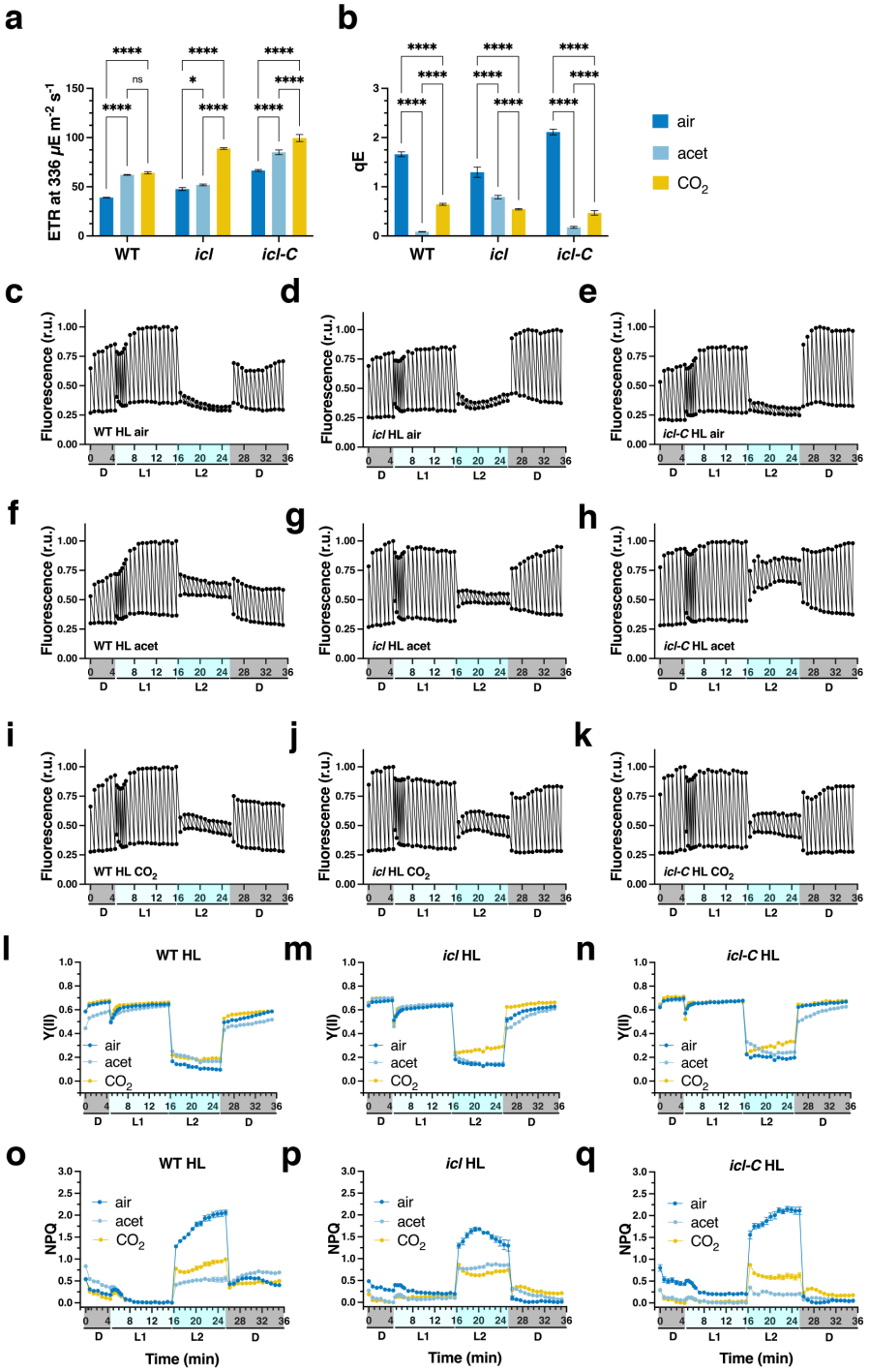

Supplementary Fig. 2: Effect of carbon availability on the photosynthetic properties of WT, *icl* and *icl-C* cells. a relative photosynthetic electron transfer rETR and **b** qE of WT, *icl* and *icl-C* cells exposed to 600 µmol photons m^{-2} s^{-1} in HSM for 4h; sparged with air (labelled as "air"); sparged with air and supplemented with 10 mM sodium acetate (labelled as "acet); sparged with air enriched with 5% CO_2 (labelled as "CO_2"). (n = 3 biological samples, mean ± s.d.). The statistical analyses (two-way anova tests) of (A) and (B) are shown in the graph; * = P value < 0.05, ***=P value <0.001. **c-k** Raw data of *in vivo* chlorophyll fluorescence (normalized to Fm) for WT, *icl* and *icl-C*. Just prior to the onset of the measurements, cells were acclimated to darkness for 15 min. Chlorophyll fluorescence was recorded in the dark (labelled as "D"), at 21 (labelled as "L1") and 336 (labelled as "L2") µmol photons m^{-2} s^{-1} as indicated in the graphs. **l-n** Y(II) values calculated as (Fm'-F)/Fm'. **o-q** NPQ values calculated as (Fm − Fm′)/Fm.

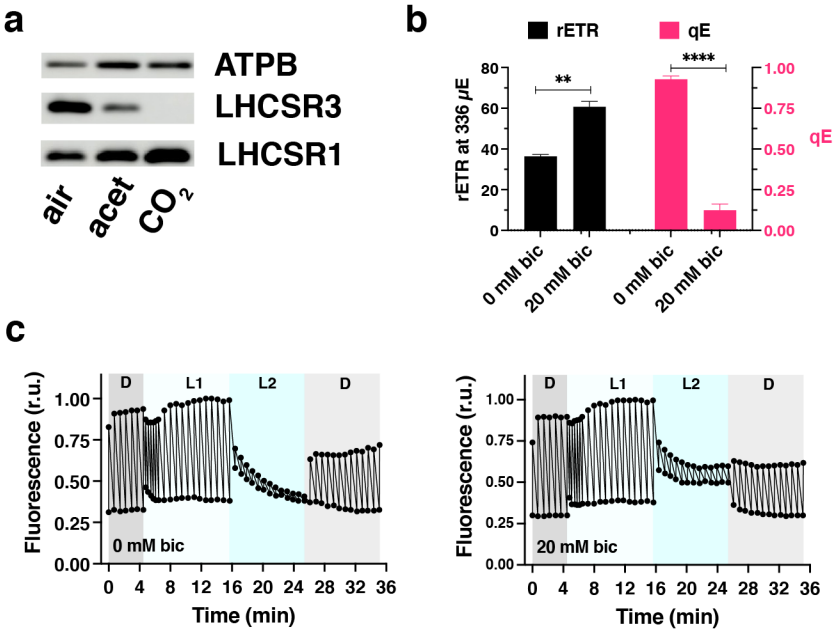

Supplementary Fig. 3: Carbon availability during the photosynthetic measurements impacts qE levels independent of the LHCSR3/1 protein levels. WT cells were acclimated for 16 h in LL (**15** µmol photons m^{-2} s^{-1}) in HSM sparged with air. After this acclimation period, light intensity was increased to 600 µmol photons m^{-2} s^{-1} (HL); samples were taken 4 h after exposure to HL. **a** Immunoblot analyses of LHCSR3, LHCSR1 and ATPB (loading control) under the indicated conditions. To facilitate direct comparison of LHCSR3 and LHCSR1 protein levels, the immunoblot analyses of LHCSR3 and ATPB shown here are the very same presented in **Fig. 1a** (HL WT panel) with the addition of LHCSR1 protein levels. **b** Relative photosynthetic electron transfer rETR and qE of WT cells exposed to HL for 4h to allow for accumulation of LHCSR1 and LHCSR3 proteins. The addition of sodium bicarbonate was done just before the photosynthetic measurements (n = 3 biological samples, mean ± s.d.). The p-values for the comparisons of rETR and qE in the absence or presence of sodium bicarbonate are based on unpaired t test with Welch's correction and are indicated in the graphs (**, P < 0.01, ****, P < 0.0001). **c** Raw data of *in vivo* chlorophyll fluorescence (normalized to Fm) used for the generation of rETR and qE graphs shown in (B). Just prior to the onset of the measurements, cells were acclimated to darkness for 15 min. Chlorophyll fluorescence was recorded in the dark (labelled as "D"), at 21 (labelled as "L1") and 336 (labelled as "L2") µmol photons m^{-2} s^{-1} as indicated in the graphs.

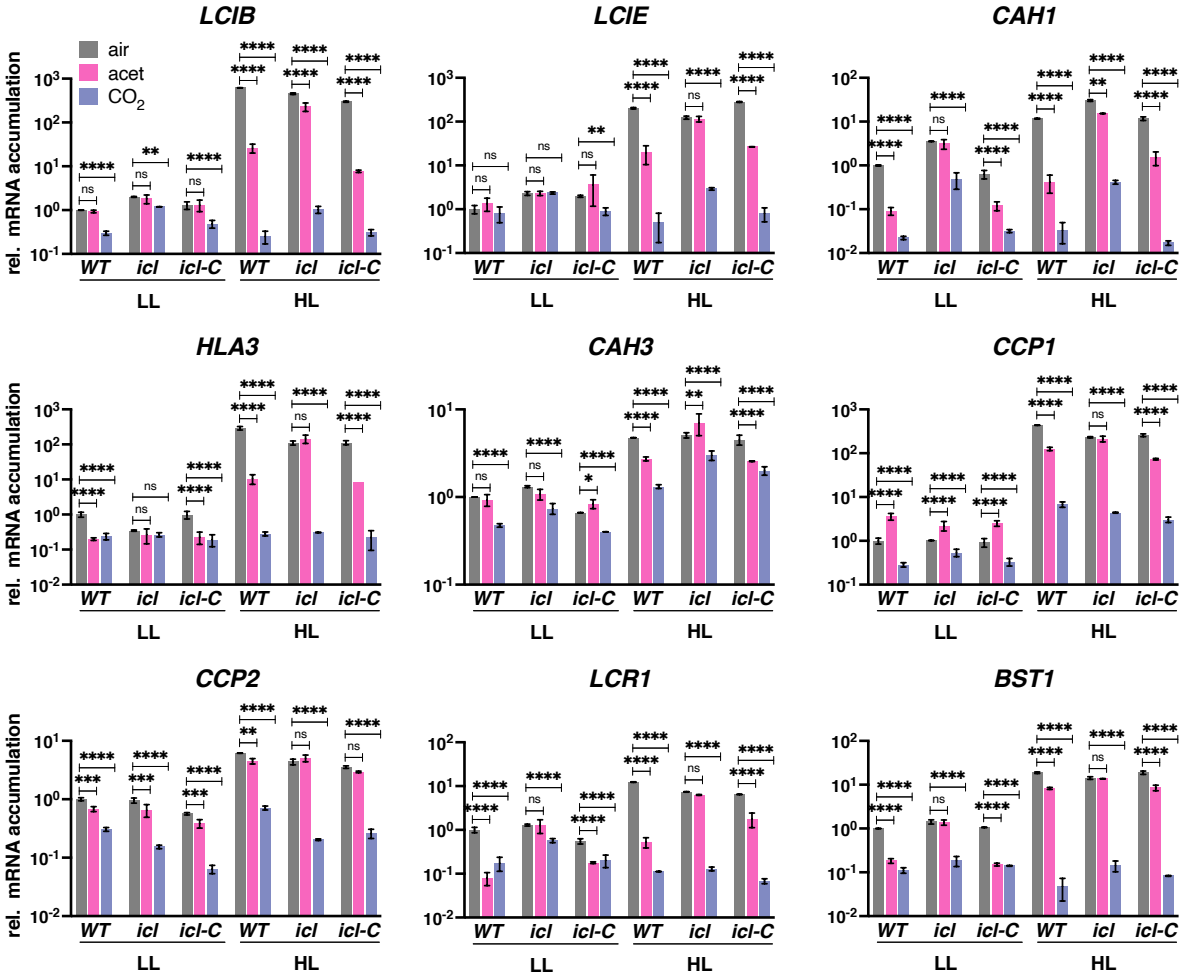

Supplementary Fig. 4: HL and low-CO_2 responses cross-talk.
WT, *icl* and *icl-C* strains were acclimated for 16 h in LL (15 µmol photons m^{-2} s^{-1}) in HSM; bubbled with air (labelled "ctrl"); bubbled with air and supplemented with 10 mM sodium acetate (labelled "acet); bubbled with air enriched with 5% CO_2 (labelled "CO_2"). After sampling for the LL conditions, light intensity was increased to 600 µmol photons m^{-2} s^{-1} (HL); samples were taken after 1h. Accumulation of mRNA of selected CCM genes at the indicated conditions normalized to WT LL ctrl. Please note that these data derive from analyses of the RNA samples of the experiment described in Fig. 1. (n = 3 biological samples, mean ± s.d.). The p-values for the comparisons of acetate and CO_2 conditions to air are based on ANOVA Dunnett's multiple comparisons test of log10 transformed mRNA data as indicated in the graphs (*, $P < 0.005$, **, $P < 0.01$, ***, $P < 0.001$, ****, $P < 0.0001$, ns, not significant).

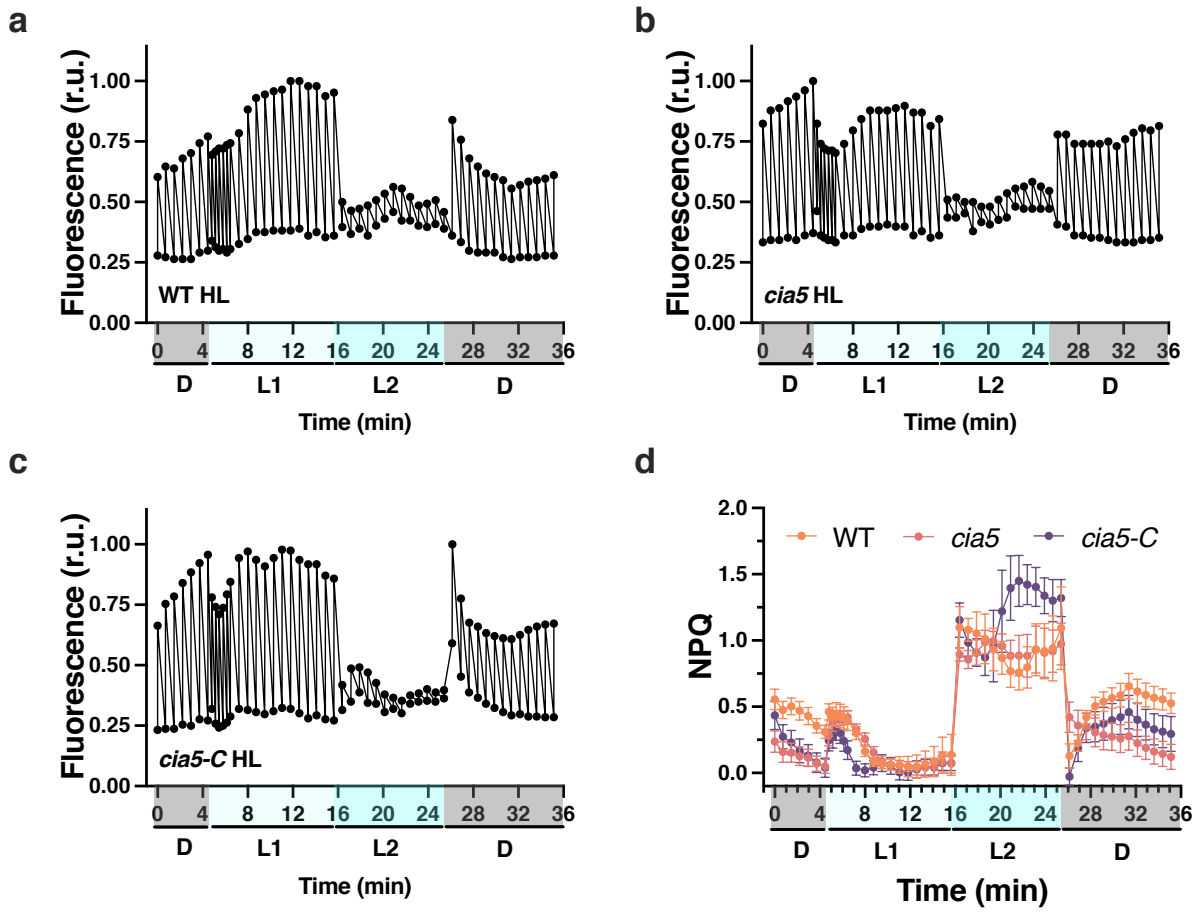

Suppementary Fig. 5: Raw data of photosynthetic measurements of Fig. 4d.
WT, *cia5* and *cia5-C* strains were acclimated for 16 h in LL (15 µmol photons m^{-2} s^{-1}) in HSM bubbled with air (labelled as "LL"); after sampling for the LL conditions, light intensity was increased to 600 µmol photons m^{-2} s^{-1} (HL); samples were taken after 4 h for photosynthesis measurements). **a-c** *In vivo* chlorophyll fluorescence (normalized to Fm) of HL-acclimated WT, *cia5* and *cia5-C* cells (for a complete description of the experimental setup please refer to the legend of **Fig. 4**. Just prior to the onset of the measurements, cells were acclimated to darkness for 15 min. Chlorophyll fluorescence was recorded in the dark (labelled as "D"), at 21 (labelled as "L1") and 336 (labelled as "L2") µmol photons m^{-2} s^{-1} as indicated in the graphs. **d** NPQ values calculated as $(Fm - Fm')/Fm'$ ($n = 3$ biological samples, mean ± s.d.).

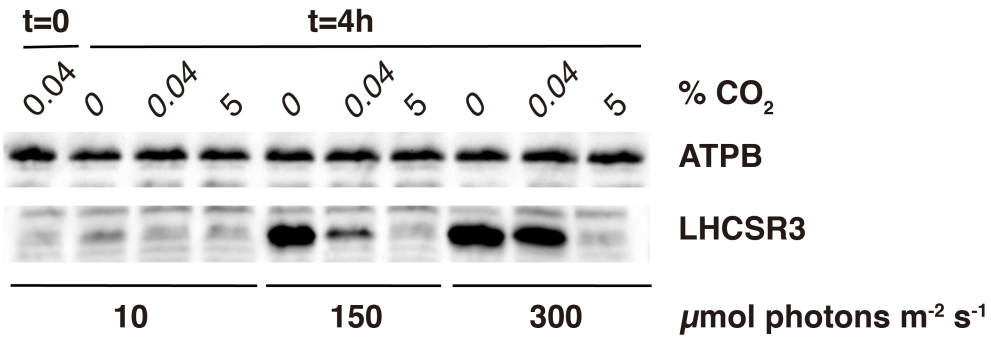

Supplementary Fig. 6: Light and CO_2 availability define expression levels of LHCSR3. WT cells, acclimated in LL (10 µmol photons m^{-2} s^{-1}) sparged with air were shifted to 10, 150, and 300 µmol photons m^{-2} s^{-1} of light and were sparged with 0 (100% O_2), 0.04 (air), and 5% CO_2 (95% O_2) for 4 hours. Shown are the immunoblot analyses of LHCSR3 and ATPB (loading control) under the indicated conditions.

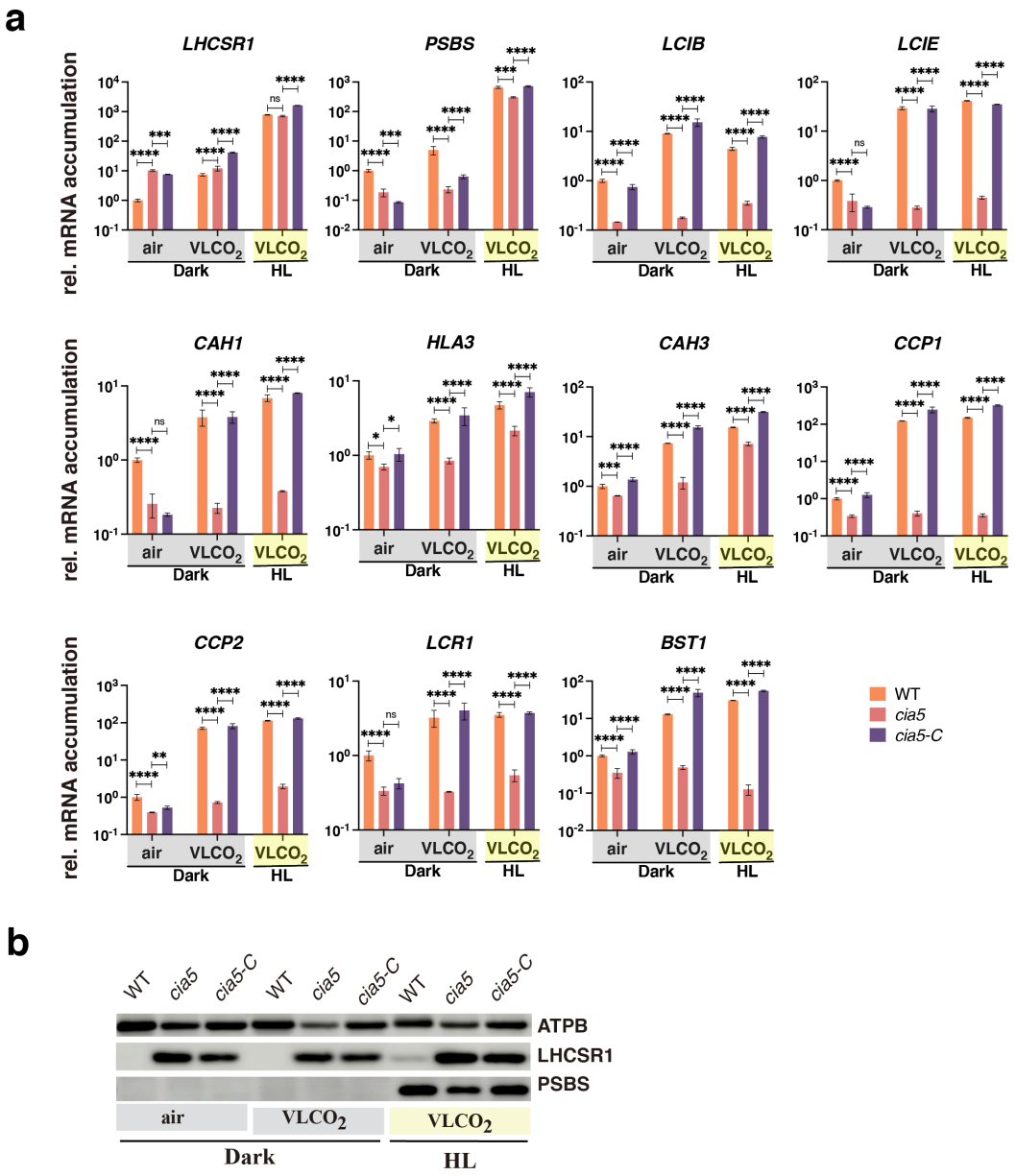

Supplementary Fig. 7: Low CO_2 levels can trigger CCM genes in the absence of light. WT, *cia5* and *cia5-C* cells were bubbled with air overnight in darkness; next day air bubbling was either maintained or replaced by CO_2-limited-air bubbling in the darkness or in the presence of 600 µmol photons m^{-2} s^{-1} light. Sampling was performed after 1 h (RNA) or 4 h (protein). **a** mRNA accumulation of *LHCSR1* and PSBS1 (qE genes) and *LCIB, LCIE, CAH1, HLA3, CAH3, CCP1, CCP2, LCR1, BST1* (CCM genes) in WT, *cia5* and *cia5-C*. Data were normalized to WT air dark; (*n* = 3 biological samples, mean ± s.d.). The p-values for the comparisons of WT with *cia5* and *cia5* with *cia5-C* are based on ANOVA Dunnett's multiple comparisons test of log10 transformed mRNA data as indicated in the graphs (*, P < 0.005, **, P < 0.01, ***, P < 0.001, ****, P < 0.0001, ns, not significant). **b** Immunoblot analyses of LHCSR1, PSBS and ATPB (loading control) under the indicated conditions.

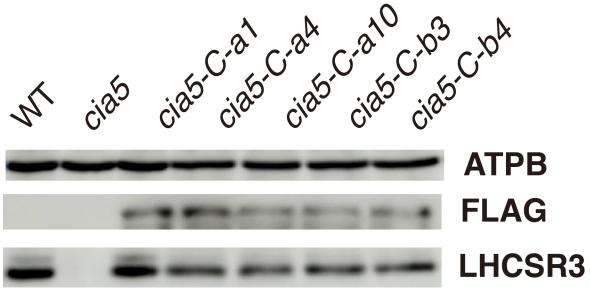

Supplementary Fig. 8: Complementation of *cia5* mutant. Immunoblot analyses of LHCSR3, FLAG and ATPB (loading control) from whole cell extracts of WT, *cia5* and four *cia5-C* complemented lines after exposure at 300 µmol photons m^{-2} s^{-1} for 4 hours.

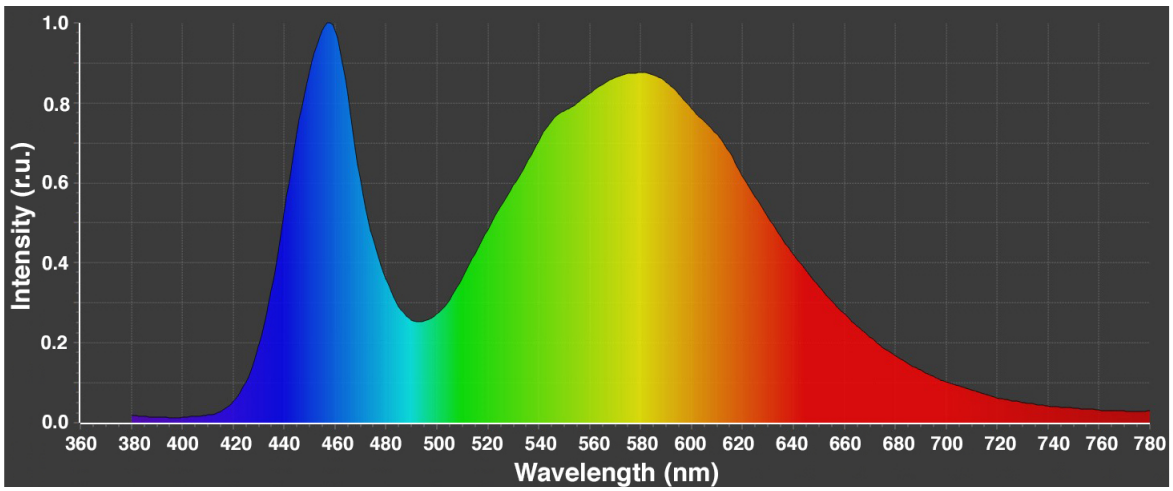

Supplementary Figure 9: Light Spectrum of the LED light system (Neptune L.E.D., France) used in the present study.

Supplementary Table 1. Predicted and observed generation time [h] for wild type and mutant strains under different growth conditions.

The wild type and mutant strains were grown photoautotrophically under low light (LL) and high light (HL) conditions and cells grown mixotroph on HSM medium supplemented with acetate under high light (HL + acetate) conditions. Values followed by an asterisk represent constraints based on measurements, the rest of the values were simulated.

	LL	**HL**	**HL + acetate**
WT	36*	20*	11
icl	36	20	19
dum11	36	22	19

Supplementary Table 2. Overview number of reactions producing CO_2 with significant changes in flux between mutants (*icl* and *dum11*) and WT. (A) Across all model reactions; (B-D) compartment-specific reactions producing CO_2 - (B) cytosol, (C) chloroplast, (D) mitochondria. A significant enrichment in reactions with flux differences between mutants and WT for reactions that produce CO2 under HL + acetate conditions only was observed considering reactions in the chloroplast and considering all model.

A – all model reactions

	CO_2 producing	not CO_2 producing	p-value
LL condition			
change in flux	24	499	0.13
no change in flux	64	1807	
HL condition			
change in flux	19	504	0.57
no change in flux	69	1802	
HL + acetate condition			
change in flux	59	1186	**0.003**
no change in flux	29	1120	

B - cytosol

	CO_2 producing	not CO_2 producing	p-value
LL condition			
change in flux	7	313	0.48
no change in flux	24	1192	
HL condition			
change in flux	7	318	0.49
no change in flux	24	1187	
HL + acetate condition			
change in flux	18	840	0.48
no change in flux	13	665	

C - chloroplast

	CO_2 producing	not CO_2 producing	p-value
LL condition			
change in flux	9	71	0.37
no change in flux	21	206	
HL condition			
change in flux	8	68	0.48
no change in flux	22	209	
HL + acetate condition			
change in flux	24	133	**6.4e-04**
no change in flux	6	144	

D - mitochondria

	CO_2 producing	not CO_2 producing	p-value
LL condition			
change in flux	8	80	0.45
no change in flux	17	198	
HL condition			
change in flux	4	70	0.9
no change in flux	21	208	
HL + acetate condition			
change in flux	17	138	0.06
no change in flux	8	140	

Supplementary Table 3. RT-qPCR primers for the genes analyzed in this study

Gene ID	Gene Name	Sense Primer	Anti-sense Primer
Cre01.g016600	PSBS1	TAAACCGTGTATTGGAACTCCG	CTCTGCACGCGGCGTGTT
Cre08.g367500	LHCSR3.1	CACAACACCTTGATGCGAGATG	CCGTGTCTTGTCAGTCCCTG
Cre08.g365900	LHCSR1	GAGTCTGAGATCACCCACGG	CCGATCTGCTGGAAGTGGTA
Cre06.g278222	GBLP	TGGCTTTCTCGGTGGACAAC	CTCGCCAATGGTGTACTTGC
Cre06.g309000	LCIA	AGATTTGATAACGGCAGGACC	CCTATCCCATGTCATTCCCAC
Cre10.g452800	LCIB	TGCATAAGAGCGGATGTAGC	CGGTAGTCAGCATCAGTCATC
Cre04.g223250	LCIE	TGCCGCCATAGATGTTGTGT	CCGCTCTTCTCTTTCGCTCA
Cre09.g399552	LCR1	GCACCAGCATACACCAAAATC	CAGAAAACAGAACGACCAAAGC
Cre03.g162800	LCI1	TTGCGGTTTTTGTACGAGCG	GTGCAAAGCCACGTCATCTC
Cre02.g097800	HLA3	CAGTGGCATGTTCCCTTTTG	GGTGCTCATGGTTCTTGTTTG
Cre03.g162800	CAH1	GCTTTGCTTCACGGTTTGGT	CCGGTACTGTGTGTATGCGT
Cre09.g415700	CAH3	AACCTGGAAGGGTGTGTGTG	CACTTCTCGAAGCTGCCGTA
Cre05.g248400	CAH4	CGAAAAGCTGCATGAACTCACC	GCCCGTAGGCTACAGTTTTC
Cre04.g223300	CCP1	TGGCATGACAACATGGCTCA	AGTGCATCCACTGGCTTGTT
Cre04.g222750	CCP2	AACGTGGAGCACATCTACGG	ATAAGCCGTCAAGCCTTGCT
Cre16.g662600	BST1	GCTGTGTGGCATTGAGGAGA	GGATGAGGCTGATGAGTCCG
Cre06.g284100	RHP1	GCAGTCGCAGGCAGTAACTA	CGCTTCAGCGCTCATAGAGA
gib-cia5		gctactcacaacaagcccagttATGGAAGCCTTAGACGCGC	gagccacccagatctccgttATCGCAGGACTGCAGCAG

Supplementary Data 1 (provided as Microsoft Excel file)
a Reactions whose minimum flux in the mutant was above the maximum flux of the WT (up-regulation) or the maximum flux in the mutant was below the minimum observed in the WT (down-regulation). Marked cells for down regulation under HL + acetate represent reactions also down regulated under LL in *dum11*. **b** Flux ranges obtained from flux variability analysis as well as mean and median flux from sampling of 5000 flux distributions. Reactions marked in green show significant difference under HL+acetate but not under LL and HL conditions.